Electron-impact excitation of the potassium atom

James O. Phelps, Jerry E. Solomon,* Dale F. Korff,† and Chun C. Lin

Department of Physics, University of Wisconsin, Madison, Wisconsin 53706

Edward T. P. Lee

Air Force Geophysics Laboratory, Bedford, Massachusetts 01730

(Received 18 April 1979)

Absolute optical electron-impact excitation functions for 24 transitions of the sharp, principal, diffuse, and fundamental spectral series of potassium have been measured. The determination of the density of the potassium vapor in the collision chamber was made by measuring the degree of transmission, by the vapor, of potassium resonance radiation generated externally in a fluorescence cell. From the measured optical excitation functions direct excitation functions have been determined for 14 states (5S, 6S, 7S, 8S, 4P, 5P, 6P, 7P, 3D, 5D, 6D, 5F, 6F, and 7F) with the aid of known radiative-transition probabilities compiled in the literature. Theoretical calculations of these same 14 excitation functions, as well as 4D and 4F, were carried out by means of the Born approximation. The 4P, 5P, 5S, 3D, and 4D direct excitation functions at intermediate energies (10–25 eV) were also calculated by the method of multistate close coupling, neglecting projectile–target-electron exchange. The high-energy (above 100 eV) Born-approximation cross sections agree with the experimental results for 4P and for all S states, but are lower than experimental results, by 30–40%, for the D and F states. At intermediate energies the close-coupling excitation calculations agree well with the experimental excitation functions for 4P and 5P, but are significantly higher than experimental values for 5S and 3D. The discrepancies between the experimental and theoretical results are probably due to a combination of systematic experimental errors, errors in the available transition-probability values, and errors in the theoretical excitation functions introduced by the use of approximate excited-state wave functions (Hartree-Fock-Slater), or, in the case of intermediate or low energies, by the neglect of projectile–target-electron exchange. The polarization of the 4P-4S and 3D-4P radiation produced by electron impact was measured, and the results were used to determine the direct excitation functions of the separate magnetic sublevels of the 4P state.

I. INTRODUCTION

The subject of electron excitation of atoms has been of interest for many years.[1] The very extensive works on helium have provided the foundation for understanding the behavior of the excitation functions in terms of the LS-coupling quantum numbers of the excited states.[1-3] This scheme of characterization of excitation functions according to the LS quantum number has been extended to neon and argon.[4,5] For these two noble-gas atoms, measurement of excitation functions has been made for over a hundred states. The shape of the excitation functions and the relative magnitude of the excitation cross sections can be successfully explained, on a qualitative level, by an extension of the scheme developed for helium.[4,5] A quantitative comparison of the experimental excitation cross sections with theory, however, is complicated by the lack of accurate wave functions for neon and argon. For an excited configuration such as $2p^5 nl$ and $3p^5 nl$ the coupling between the various angular momenta is of the intermediate type so that a first-principles treatment of the spin-orbit and spin-spin coupling is very difficult. Furthermore, there is also the possibility of substantial configuration mixing for some of the ex-

cited states. In Refs. 4 and 5 a set of semiempirical wave functions based on the work of Cowan and Andrew[6] were used. These wave functions are adequate for comparing the relative magnitude of the excitation cross sections on a semiquantitative level but not sufficiently accurate to give reliable absolute cross sections from first-principles theoretical calculations.

For quantitative study of electron excitation beyond helium, an obvious choice is the alkali-metal atoms. Here more accurate wave functions for the excited states are readily obtainable. Also because of the rather simple one-electron-type energy-level pattern as shown in Fig. 1, complete cascade corrections can be made to the apparent excitation functions for nearly all the S, P, and D series to yield direct excitation cross sections (see Sec. V). Against these advantages are the complications in the construction of the apparatus caused by the chemical activity of the alkali-metal atoms and, more seriously, the difficulty of accurate determination of the vapor density of the atoms in the collision chamber. The latter point is discussed in Sec. III. Measurements of electron excitation cross sections for the alkali-metal atoms have been reported in the literature as early as the 1930s.[7] Studies of numerous levels of the
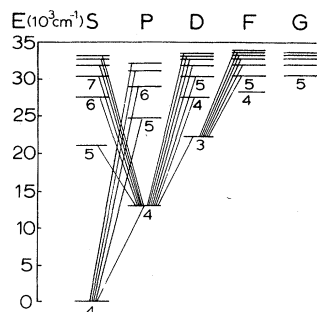
FIG. 1. Energy levels of potassium. The transitions observed in the present experiment are indicated by lines joining the levels. No transitions were studied involving the $4F$ nor any of the G states.

FIG. 2. Schematic diagram of apparatus. Lenses are indicated by the usual symbol, such as the one marked "L" at the top of the drawing. Mirrors are indicated by diagonal lines, such as the one marked "M," solid if fixed, dashed if removable. Collision-chamber windows and compensating windows are marked W. "Thru" and "Bypass" identify the two alternate optical paths for light from the resonance lamp. The potassium reservoir is marked "K."

alkali metals were done by Zapesochnyi *et al.* in the 1960s; their work and that of others done prior to 1968 is summarized in Ref. 1. Since then, Zapesochnyi, Postoi, and Aleksakhin,[8] using a crossed-beam technique, have remeasured a number of cross sections with results that are in considerable disagreement with the earlier work. It has been suggested that the latter may be in considerable error because of faulty number-density determination.[1,8] Gallagher and his co-workers have recently completed measurements of the excitation functions of the resonance lines of all alkali metals.[9-11] The incident energy in their experiment extends up to 1500 eV, and the absolute cross sections are obtained by normalizing the experimental data for relative cross sections to theoretical values obtained by the Born approximation in the high-energy range so that the atom number density need not be known. In many cases their results do not confirm those of previous workers. Thus a reasonable concensus on experimentally measured alkali-metal excitation functions has not yet been reached.

In this paper we report a comprehensive study of electron excitation of the S, P, D, and F states of the potassium atom. We choose potassium because experimentally it is easier to work with than sodium and yet the theoretical analyses are not much more complicated. The vapor density is determined experimentally by measuring the attenuation of the $4P$-$4S$ radiation from a potassium fluorescence cell so that the absolute cross sections are obtained entirely by experimental means. Theoretical calculations of the excitation cross sections are made by using the Born approximation and the more refined method of close coupling, and the results are compared with the experimental data.
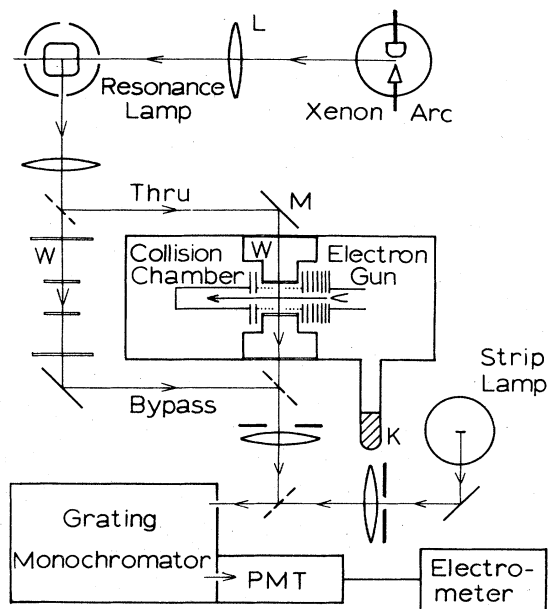
II. EXPERIMENTAL PROCEDURE

A block diagram of the apparatus is shown in Fig. 2. Potassium vapor is evaporated from a small sidearm into an evacuated collision chamber. Here a collimated beam of monoenergetic electrons passes through the gas and excites some of the atoms upon impact. This excitation process is studied by observing the radiation that is emitted by the excited atoms into a direction perpendicular to the beam. The light emerging from the collision chamber is focused by a lens onto the entrance slit of a monochromator where it is dispersed and then detected by a photomultiplier, which is calibrated against a strip-lamp pyrometer. The output of the photomultiplier is measured with an electrometer and plotted as a function of electron-beam energy on an X-Y recorder. The xenon arc and resonance lamp in the upper part of the figure are used for determining the potassium vapor density in the collision chamber. This will be discussed in Sec. III.

Details of operation of the experiment are as follows. The potassium was introduced into the sidearm under a vacuum of 10^{-6} Torr, after the collision chamber had been baked out at 400 °C.
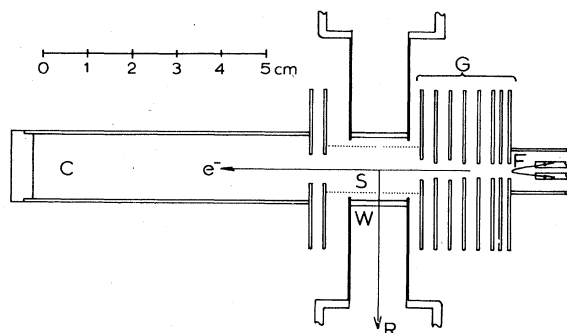
FIG. 3. Detail of collision region, electron gun, and windows. e^-, electron-beam axis; R, optical axis for electron-impact radiation; W, sapphire windows; S, wire shield and collision region; C, electron-beam collection cup; F, electron-gun filament; G, electron-gun grids.

The potassium vapor in the collision chamber was found by spectroscopic analysis to contain approximately 0.08% Na, 0.17% Rb, and 0.04% Cs by number density, a level of impurities we believe to be of no consequence. The vapor density is varied within the range of 10^{10}–10^{13} atoms/cm^3 by setting the temperature in the sidearm between 60° and 145 °C while holding the temperature of the collision chamber at a constant 200 °C. The collision chamber, of type-304 stainless steel, is continuously pumped through a high impedance to prevent the accumulation of leakage or outgas impurities. The background pressure is 10^{-7} to 10^{-6} Torr.

The collision region and electron gun are shown to scale in Fig. 3. The gun, an elaboration on the Pierce design, was constructed from commercially supplied stainless-steel and alumina parts. In operation, electrons emitted from a thoriated tungsten filament are accelerated and focused into the collision region. This region is enclosed by windings of fine tungsten wire, an arrangement which provides adequate electrostatic shielding without interfering with the free flow of potassium atoms nor with the diffusion of resonance radiation. The beam traverses this region, then passes through an exit aperture and into the collection cup. The energy range is zero to 400 eV, with a resolution of about 0.75 eV full width at half maximum (FWHM) as determined by analysis of sharpness and steepness of ascent of the excitation-function data in the vicinity of onset. The beam current is varied between zero and 30 μA, over which range the excitation signal was found to vary proportionally with beam current. The beam diameter is typically 3 mm and the maximum possible half angle of divergence was limited to 6° by the apertures of the gun. The electron currents collected by the cup and by the

exit aperture plate of the collision region are measured simultaneously, and the focusing so adjusted that the ratio of the former current to the latter is maximized, typically 20:1. The beam collimation is further analyzed by measuring the intensity of optical excitation as a function of position across a diameter of the beam. Proper electron-beam collimation is necessary in order to ensure that an entire cross-sectional slice of the beam lies within the field of view of the optical detection system, and to hold to a minimum the number of secondary electrons in the collision region. Such electrons, produced when the beam strikes surfaces in the immediate vicinity of the collision region, cause a distortion of the apparent excitation function. [1,8]

The inner windows of the collision chamber are of sapphire, chosen because of its resistance to attack by hot alkali-metal vapor and because of its transparency over a broad range of wavelengths. The surfaces of the windows are perpendicular to the c axis of the crystal, thereby preventing alteration of the polarization of the radiation as it passes normally through the window. They are recessed well into the collision chamber, to within 7 mm of the electron-beam axis, in order to reduce the path length for scattering of resonance radiation. Outer windows of fused quartz are also used and the intervening space is evacuated, forming a double vacuum seal. This eliminates convective cooling of the inner windows, and also prevents any possible leakage by the sapphire-Kovar seal, which is subject to substantial thermal cycling.

The grating monochromator is of the Ebert-Fastie type, having a focal length of 0.5 m and a focal ratio of $f/8.6$. The position of the monochromator along the optical axis of the experiment is varied as a function of wavelength, to accommodate the chromatic aberration by the quartz imaging lens. The monochromator slits are perpendicular to the electron beam and are opened to give a passband of approximately 8 Å.

Two types of photomultiplier are used: a gallium arsenide RCA C31034-A for wavelengths below 8700 Å and an S-1 RCA 7102 for wavelengths above. These are operated at temperatures of −20 and −80 °C, respectively, reducing the dark current to a small fraction of all but the weakest signals. A Fabry lens is used to defocus the light falling on the photocathode.

The radiometric standard is a GE 20A/T24/2 tungsten strip-lamp pyrometer, whose temperature calibration has recently been verified to within 3.5 °C by a local standards laboratory. The lamp is operated at true temperatures of 1400, 1600, and 2000 K. The values assumed for the

spectral emissivity of the tungsten ribbon are those of DeVos.[12] Care is taken to exclude spurious reflections from within the strip lamp. Nearly identical lenses, mirrors, and optical paths are used for the excitation light and the strip-lamp light, only the aperture stops and source windows being different. The direct proportionality of the photomultiplier signal to the aperture-stop area is verified experimentally.

Precautions are taken to ensure that the strip-lamp light, after emerging from the monochromator, is of adequate spectral purity. During calibration in the violet and near-ultraviolet region, the principal spectral contaminant is stray light from the near infrared, where the strip-lamp radiance is very high. This scattered light can be eliminated most simply by the use of colored glass filters such as Corning CS 7-37, 5-58, and 4-96. At the other extreme, beyond 12 000 Å, calibration is hampered by stray light from the wavelength range 6000–10 500 Å, where the S-1 photocathode's sensitivity is far greater than at 12 000 Å. This is eliminated by using one or two thicknesses of Kodak Wratten filter 87-A. Second orders are eliminated with Corning filter CS 2-59.

Polarization components consist of Polaroid filters HNP'B, HN-32, or HR placed in front of the spectrometer entrance slit and oriented manually. The strip lamp is used as a source of zero polarization, against which polarization of the lines is measured. Polarization effects are considered for two reasons. First, the polarization of a line is of theoretical interest for, among other reasons, the information it provides about the excitation of the separate magnetic sublevels of the atom.[13] This topic will be discussed in Sec. VI. Second, the polarization of a line is related to the angular distribution of the emission.[1] In order to determine the total excitation cross section of a line it is necessary to deduce the integral of the radiant intensity over all solid angles, based upon measurements of the intensity at a single, fixed, observation angle, i.e., 90° to the electron beam. If the polarization of a line is very small, as we have found with the sharp series and the higher members of the other series, then the emission is nearly isotropic and the angular integration becomes trivial. In other cases, notably the lower few members of the three other series, the polarization may reach 25% or more, indicating measurable anisotropy of emission. In these cases use is made of the fact that the intensity of dipole radiation emitted at right angles to the axis of quantization and having its electric vector oriented at 54.8° to that axis is proportional to the total radiation emitted into all directions, regardless

of the angular distribution, or equivalently, the polarization of the emitted line.[1] Thus, in principle, the use of a polarizer in this "magic-angle" orientation effectively carries out the angular integration of the intensity; moreover, by presenting a constant plane of polarization to the monochromator, it prevents distortions in the excitation functions resulting from the polarizing properties of the monochromator. However, the use of the polarizer also weakens the signal significantly—by a factor of 4, typically. Thus its use was restricted to the stronger lines. Since these happen to include the most strongly polarized lines, the largest polarization related errors are eliminated.

In carrying out the experiment each excitation function was examined immediately after the corresponding radiometric calibration was made, so as to reduce the effects of any drifting in the detector sensitivity. The various excitation functions were measured in rapid sequence, throughout which as many experimental parameters as possible were kept constant, e.g., spectrometer slit widths, aperture areas, beam current, etc. The number density was checked at regular intervals during each sequence. Our final results are based upon several of these data runs.

III. DETERMINATION OF ATOM NUMBER DENSITY

In order to obtain absolute excitation functions it is necessary either to normalize them to some known value, or else to have complete knowledge of all appropriate experimental parameters, including the number density of atoms in the collision region. In the case of normalization a common choice for the "known" cross section is that computed by using the Born approximation. The approximation made in that calculation is considered to be valid at sufficiently high energies, but even then the accuracy of the final result depends upon the quality of the ground- and excited-state wave functions employed and is difficult to assess. For this and other reasons, differences ranging from a few percent to a factor of 2 or more in calculated cross sections are found in the literature,[14] complicating the choice of a "known" cross section to which experimental results are to be normalized. Also, at the high energies required for Born normalization, many of the excitation signals are too weak to be measured with sufficient precision. Finally we find it more satisfying to determine the cross sections based entirely on experimental measurements. For these reasons we have chosen not to use such normalization procedures and have included number-density determination in our experiment.

The method of obtaining alkali-metal vapor number-density used by previous workers in static-gas experiments such as ours consists of measuring the temperature of the potassium reservoir and then obtaining the corresponding equilibrium vapor pressure from standard literature sources. However, at some of the lower densities used in our experiment (e.g., $N = 2 \times 10^{10}$ cm^{-3}), the attainment of thermodynamic equilibrium is highly problematic because of the chemical activity of the vapor and its adsorption and desorption by the walls. The coating of the walls with potassium droplets, in an effort to ensure vapor-pressure saturation, is not applicable due to the presence of insulating parts of the gun, windows, etc. In addition to these problems there is disagreement among vapor-pressure values cited in the literature,[15,16] amounting to 25% in the density range of interest.

To avoid these difficulties, we have used instead the resonance-transmission method, in which the vapor density in the collision region is determined by measuring the degree of transmission, by the vapor, of potassium resonance radiation. The radiation is generated externally in a potassium fluorescence cell, which is simply a small, permanently sealed Pyrex cell of square cross section, which is evacuated except for a small quantity of potassium. A potassium vapor density of approximately 2×10^{10} cm^{-3} is maintained in the cell by holding it at a constant temperature of 60 °C. The $4P$ resonance levels of this vapor are excited by illuminating the cell with intense continuum radiation from a high-pressure xenon arc and in the subsequent radiative decay the desired potassium resonance lines are emitted. We used the D-1 line, resulting from the $4P_{1/2} \rightarrow 4S_{1/2}$ transition and having a wavelength of 7699 Å. This light is directed along either of two similar paths (Fig. 2), one passing through the collision chamber and the other around it. The integrated transmittance of the line by the vapor in the collision chamber is readily obtained by comparing the intensities of these two beams.

From the integrated transmittance T of the resonance line by the vapor, the number density N in the collision chamber is deduced. This step requires that the functional relationship between T, N, and the absorption path length L be known. This was obtained in the following way. If the emission profile of the source is denoted by $I(\bar{\nu})$ and the absorption cross section of the absorbing vapor by $K(\bar{\nu})$ where $\bar{\nu}$ is the wave number, then

$$T(NL) = \frac{\int I(\bar{\nu}) e^{-NLK(\bar{\nu})} \, d\bar{\nu}}{\int I(\bar{\nu}) d\bar{\nu}} . \qquad (1)$$

Thus to compute $T(NL)$ we need to know both $I(\bar{\nu})$ of the source and $K(\bar{\nu})$ of the absorber.

The effective absorption cross section of the vapor is a weighted superposition of several unresolved isotopic and hyperfine components $K_{FF'A}(\bar{\nu})$,

$$K(\bar{\nu}) = \sum_{F} \sum_{F'} \sum_{A} N_A W_F K_{FF'A}(\bar{\nu}) , \qquad (2)$$

where A is the atomic weight of the isotope, and F and F' are the total angular momenta (nuclear plus electronic) of the hyperfine substates of the ground electronic state $(4S_{1/2})$ and the excited electronic state $(4P_{1/2})$, respectively. The weighting factor N_A is the fraction of atoms of isotope A; there are two stable isotopes of potassium, $A = 39$ and 41, and we assume they are present in their natural isotopic abundances $N_{39} = 0.934$ and $N_{41} = 0.066$. The two isotopes have the same nuclear spin $I = \frac{3}{2}$, so the possible values for the total angular momentum are $F = 1, 2$ and $F' = 1, 2$ for both of them. The weighting factor W_F in Eq. (2) is the fraction of ground-state atoms with total angular momentum F and we assume it to be proportional to the statistical weight $2F + 1$ so that $W_1 = \frac{3}{8}$ and $W_2 = \frac{5}{8}$. Thus the sum (2) contains eight components, each of which is subject to the normalization condition expressed by the Fuechtbauer-Ladenburg equation,[17]

$$\int K_{FF'A}(\bar{\nu}) d\bar{\nu} = \pi r_e f_{FF'} , \qquad (3)$$

where r_e is the classical electron radius and $f_{FF'}$ is the absorption oscillator strength of the FF' hyperfine component of the D-1 line. Denoting the oscillator strength of the entire D-1 line simply by f, we obtain, by applying standard Russell-Saunders coupling formulas, $f_{11} = \frac{1}{6}f$, $f_{12} = \frac{5}{6}f$, and $f_{21} = f_{22} = \frac{1}{2}f$.[18]

Each of the line components is subject to two kinds of broadening, namely, Doppler broadening and, to a much lesser extent, natural broadening. Thus each component has a Voigt profile,[17] i.e., a convolution between a Gaussian, having a FWHM of $2\sqrt{2\ln 2}\,\sigma_A$, and a Lorentzian, having a natural width Γ(FWHM), centered about some wave number $\nu_{FF'A}$. Here σ_A is the Doppler parameter given by

$$\sigma_A = (1/\lambda)(RT/M_A c^2)^{1/2} , \qquad (4)$$

where λ is the wavelength, R is the gas constant, T is the absolute temperature, M_A is the isotopic mass, and c is the speed of light. These Voigt functions, denoted by $U_{FF'A}(\bar{\nu})$, are normalized so that

$$\int U_{FF'A}(\bar{\nu}) d\bar{\nu} = 1. \qquad (5)$$

The total effective absorption cross section of the

D-1 line is then

$$K(\bar{\nu}) = \sum_F \sum_{F'} \sum_A \pi r_e f_{FF'} N_A U_{FF'A}(\bar{\nu}) . \qquad (6)$$

In calculating this function, we used the values $f = 0.339$, and $\Gamma = 0.20 \times 10^{-3}$ cm^{-1}.[19] The central wave numbers $\bar{\nu}_{FF'A}$ of the various components, relative to the centroid of the total line, in units of 10^{-3} cm^{-1} are $\bar{\nu}_{1,1,39} = 7.9$, $\bar{\nu}_{2,1,39} = -7.5$, $\bar{\nu}_{1,2,39} = 9.9$, $\bar{\nu}_{2,2,39} = -5.5$, $\bar{\nu}_{1,1,41} = 12.3$, $\bar{\nu}_{2,1,41} = 3.8$, $\bar{\nu}_{1,2,41} = 12.3$, and $\bar{\nu}_{2,2,41} = 3.8$.[20,21] The computation of the Voigt profile is carried out on a computer following the method of Hummer.[22]

The emission profile $I(\bar{\nu})$ of the resonance lamp is computed in exactly the same way except that the lamp temperature of 60 °C is used in place of the collision-chamber temperature of 200 °C in computing the Doppler width. The simple fact that the emission profile of the vapor in the lamp is identical to its absorption profile is a result of the nature of the xenon arc light that excites the resonance lamp. Viewed with a resolution of 0.2 Å the xenon arc spectrum shows no detailed structure in the vicinity of the D-1 line other than a gradual rate of change of 0.18% per cm^{-1} or 0.007% over the FWHM of the D-1 line. It is reasonable to assume that this uniformity continues on a finer scale than this in view of the high operating pressure and temperature of the arc (50–70 atm, several thousand degrees K). Thus the exciting light may be considered to be "white." This produces "natural" excitation of the potassium vapor, under which circumstance its emission profile is identical to its absorption profile, for all directions of emission.[18] The emission is also un-

FIG. 4. Transmittance of potassium D-1 radiation $(4P_{1/2}$-$4S_{1/2})$ by a layer of NL potassium atoms/cm^2. The temperature of the source is 60 °C, that of the absorbing layer 200 °C.

polarized.

The results of the calculation of $T(NL)$ are displayed in Fig. 4. Further corrections were made to take account of the internal reflections within the collision chamber and resonance lamp and the effects of departures from whiteness of the exciting light, caused by its absorption within the lamp. These corrections are small, and are not presented in Fig. 4, since they are peculiar to the particular geometrical arrangement employed and not of general interest.

The range of applicability of the calculated $T(NL)$ is restricted by the model used in the calculation and by practical considerations. At high densities, the transmitted radiation not only becomes weak and therefore difficult to measure with precision, but also becomes dominated by increasingly remote portions of the wings of the line, where broadening mechanisms other than those considered may play a role, thus reducing the validity of our calculations. Multiple scattering of the resonance radiation within the collision chamber also becomes non-negligible. At the other extreme, i.e., at very low densities, where the transmittance approaches unity, large fractional errors in the number density can result from rather small errors in the measured transmittance. These difficulties restrict the range over which the density can be accurately determined. Practical limits for the range of NL are 2×10^{10} to 3×10^{12} cm^{-2}, which, for our path length of $L = 1.43$ cm, corresponds to a density range of 1.4×10^{10} to 2.1×10^{12} cm^{-3}. Within this range we expect the precision of the number-density determination to be 10%.

Those cross sections with the strongest signals, i.e., $4P$-$4S$, $5P$-$4S$, $6S$-$4P$, and $5D$-$4P$, were measured at densities within this optimum range. The remaining weaker lines, however, had to be studied at higher densities, up to 7×10^{12} cm^{-3}. In these cases, where the number density could not be reliably determined by the method outlined above, we measured the cross-section values relative to a fixed reference cross section Q_{6S-4P} at 15 eV. (The $6S$-$4P$ lines were chosen because they are strong and unpolarized and lie in a convenient part of the spectrum, and because they are nonresonance lines and therefore not subject to resonance absorption. Q_{6S-4P} is also well suited since it has a rather flat portion, with respect to impact energy, in the vicinity of 15 eV.) The reference cross section was then separately determined by a number of measurements made within the optimum-density range and from its value the various relative cross sections could be determined absolutely. The validity of this method requires that the ratio of the signals for
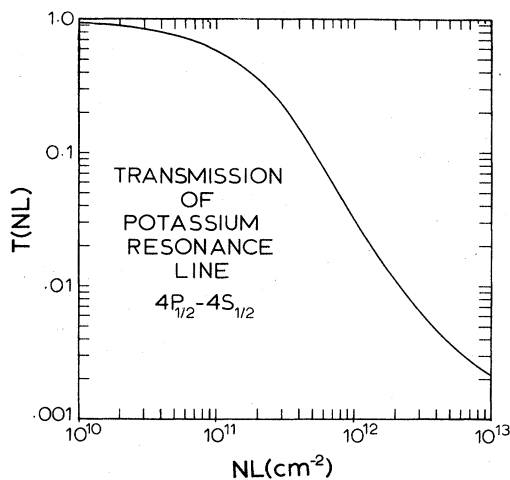
any two cross sections be independent of the number density, or, equivalently, that such nonlinear processes as collisional transfer of excitation be of negligible importance. Our data indicate that this requirement is satisfied up to the highest density used, $\sim 7 \times 10^{12}$ cm^{-3}.

IV. EXPERIMENTAL RESULTS FOR OPTICAL EXCITATION FUNCTIONS

A. General features

The optical (or line) excitation function $Q_{jk}(E)$ is defined as the cross section for production of photons associated with the $j \to k$ transition due to impact of electrons of energy E upon atoms initially in the ground state. The production includes both the direct and indirect (cascade) processes. Its dependence upon the various experimentally determined quantities is expressed by the equation

$$Q_{jk}(E) = F_{jk} S_{jk}^c I_{jk}^e(E) / N I^b I_{jk}^c, \qquad (7)$$

where $I_{jk}^e(E)$ is the photomultiplier signal produced by the $j \to k$ photons, I_{jk}^c is the photomultiplier signal produced by the strip lamp at the wavelength corresponding to the $j \to k$ transition, S_{jk}^c is the spectral radiance of the strip lamp at that wave-

length, N is the number density, I^b is the beam current, and F_{jk} is a factor which incorporates the slit width and other geometrical factors, window transmittances, etc., which are independent of energy and vary only slightly from one spectral line to the next.

We have determined the absolute optical excitation functions for the 24 transitions indicated in Fig. 1. These comprise the first several members of the sharp (nS-$4P$), principal (nP-$4S$), diffuse (nD-$4P$), and fundamental (nF-$3D$) spectral series, excepting only $4F$-$3D$, which lies beyond the infrared limit of our detector. Each transition refers to a combined spin multiplet. The cross sections for the individual lines within each multiplet were found to follow standard Russell-Saunders intensity ratios in all cases examined.

All 24 excitation functions were measured in the 0–50-eV interval and five of them ($6S$-$4P$, $4P$-$4S$, $5P$-$4S$, $3D$-$4P$, and $5D$-$4P$) were also measured in the extended range 50–400 eV. Values of these cross sections at selected energies are presented in Table I. The absolute optical excitation func-

TABLE I. Experimental optical excitation functions of potassium.

Transition j–k	Wavelength (Å)	Uncertainty (%) [a]	Cross section Q_{jk} (10^{-18} cm^2) at energy E (eV)								
			5	10	15	20	30	50	100 [b]	200 [b]	400 [b]
5S-4P	12 432–12 522	20	599	371	275	235	193	135	(87.3)	(46.0)	(23.1)
6S-4P	6 911– 6 939	12	55.9	33.8	26.1	23.3	18.9	13.8	8.27	4.36	2.19
7S-4P	5 782– 5 802	15	15.7	9.61	6.81	6.04	4.91	3.75	(2.16)	(1.14)	(0.57)
8S-4P	5 323– 5 340	15	6.14	3.80	2.69	2.47	2.11	1.56	(0.85)	(0.45)	(0.23)
9S-4P	5 084– 5 099	15	3.07	2.06	1.41	1.25	1.06	0.86	(0.45)	(0.24)	(0.12)
10S-4P	4 942– 4 956	20	1.69	1.10	0.78	0.69	0.59	0.48	(0.25)	(0.13)	(0.07)
4P-4S	7 665– 7 699	12	6020	6240	5690	5150	4300	3370	2160	1300	745
5P-4S	4 044– 4 047	15	70.8	52.4	43.1	37.3	27.9	19.9	11.6	6.33	3.34
6P-4S	3 446– 3 447	20	6.02	4.03	3.24	2.78	2.08	1.39	(0.87)	(0.48)	(0.25)
7P-4S	3 217– 3 218	20	0.82	0.53	0.43	0.36	0.27	0.20	(0.12)	(0.06)	(0.03)
8P-4S	3 102– 3 102	20	0.20	0.13	0.10	0.09	0.07	0.05	(0.03)	(0.02)	(0.01)
3D-4P	11 690–11 772	15	1280	1120	874	712	525	347	198	107	54.2
4D-4P	6 936– 6 965	15	1.02	0.71	0.52	0.41	0.30	0.20	(0.11)	(0.06)	(0.03)
5D-4P	5 812– 5 832	15	18.3	12.2	8.88	7.05	5.01	3.40	1.87	0.99	0.50
6D-4P	5 343– 5 360	15	14.8	9.22	6.73	5.35	3.85	2.63	(1.42)	(0.75)	(0.38)
7D-4P	5 097– 5 112	15	8.55	5.00	3.78	3.05	2.17	1.48	(0.80)	(0.42)	(0.21)
8D-4P	4 951– 4 965	15	5.05	2.92	2.15	1.78	1.24	0.82	(0.45)	(0.24)	(0.12)
9D-4P	4 865– 4 870	20	2.64	1.52	1.12	0.93	0.65	0.43	(0.24)	(0.12)	(0.06)
5F-3D	11 020–11 023	20	46.7	30.7	21.4	16.2	11.1	7.16	(3.74)	(1.88)	(0.94)
6F-3D	9 596– 9 598	20	21.1	13.9	9.47	7.27	5.07	3.47	(1.66)	(0.83)	(0.42)
7F-3D	8 902– 8 904	20	9.76	7.08	4.88	3.87	2.66	1.73	(0.85)	(0.43)	(0.22)
8F-3D	8 503– 8 505	15	5.82	4.06	2.82	2.15	1.50	1.00	(0.49)	(0.25)	(0.12)
9F-3D	8 250– 8 252	15	3.57	2.49	1.67	1.32	0.92	0.59	(0.29)	(0.15)	(0.07)
10F-3D	8 078– 8 080	15	2.04	1.51	1.03	0.80	0.57	0.35	(0.18)	(0.09)	(0.05)

[a] Uncertainties correspond to 70 % confidence level.
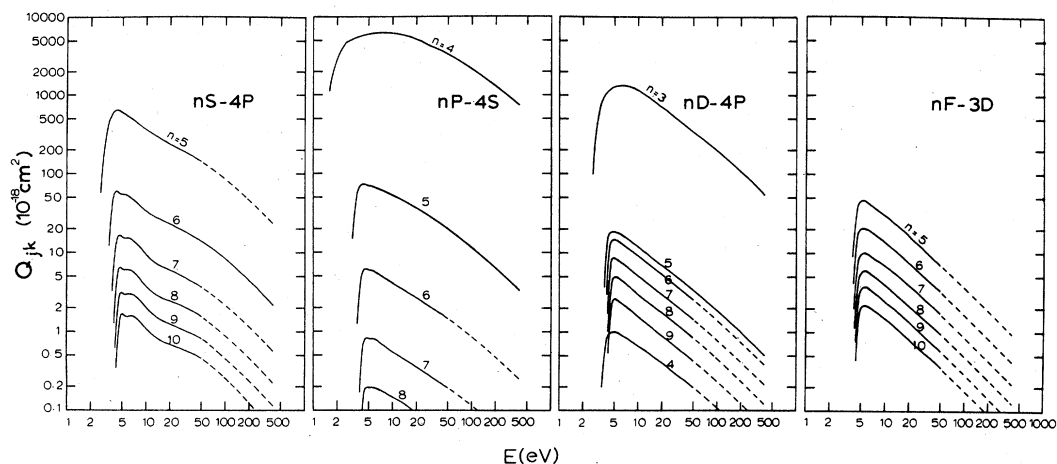[b] Values in parentheses are based upon extrapolation.

FIG. 5. Experimental optical excitation functions of potassium for sharp, principal, diffuse, and fundamental series. Solid lines indicate experimental measurements; dashed lines represent extrapolations, explained in text.

tions of all lines observed are plotted on a log-log scale in Fig. 5. The unbracketed numbers in Table I and the solid lines in Fig. 5 represent direct measurements, while the numbers in parentheses and the dashed curves are extrapolations, to be discussed shortly. The relative excitation functions (normalized to unity at $E = 15$ eV) of the first two observed members of each series are shown on a linear scale in Fig. 6 for purposes of shape comparison.

In the results presented here, the electron energy distribution has not been deconvolved from the data; thus any narrow features in the true excitation functions will appear here to be somewhat attenuated and broadened by approximately 0.75 eV, the FWHM of the beam energy distribution. Features lying within about 0.75 eV of each other are not resolved, and small, nonreproducible, or ambiguous structures have been smoothed out in the data presentation.

Several general observations regarding the magnitude and shape of potassium optical excitation functions can be made upon examining these data. From Fig. 5 it is seen that within each spectral series the cross section magnitudes at fixed energy decrease regularly with increasing principal quantum number n. The only exceptions, $4D$-$4P$ and to a lesser extent $5D$-$4P$, are due to anomalously small transition probabilities.[19] For the higher numbers of each series, i.e., excluding only the first member in each series and the two transitions cited above, this behavior can be described with an rms precision of 6.5% by the power law

$$Q_{nl-n'l'} = C_l (n_{nl}^*)^{-\alpha_l},$$

$$nl = 6S \cdots 10S, \ 5P \cdots 8P, \ 6D \cdots 9D, \ 5F \cdots 10F,$$

$$(8)$$
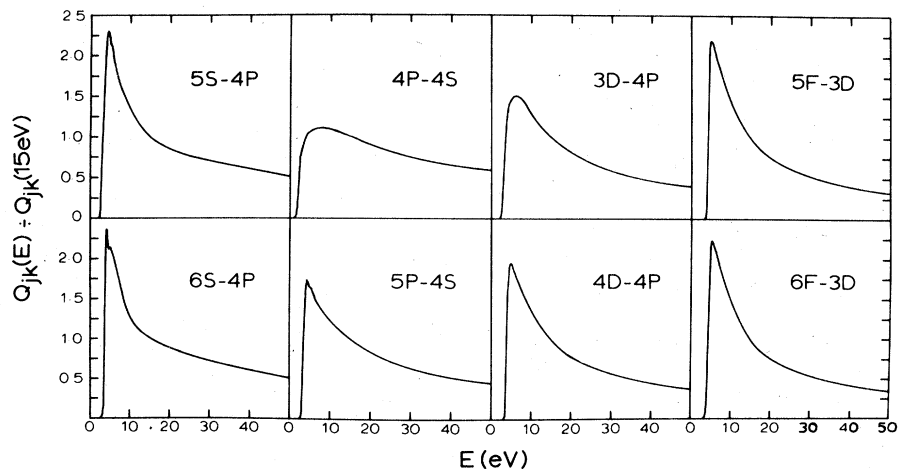
where n and l are the principal and orbital-angu-

FIG. 6. Relative optical excitation functions of the first two observed members of the sharp, principal, diffuse, and fundamental series. The curves are scaled to unity at 15 eV.

lar-momentum quantum numbers of the upper state of the transition, n' and l' are the corresponding quantities for the lower state, n_{nl}^* is the effective quantum number of the upper state determined from its energy relative to the ionization limit,[19] α_l is a constant for each spectral series, and C_l is a function of impact energy and is different for each spectral series. At an impact energy of 15 eV, values of α_l and of C_l (in units of 10^{-18} cm^2) are $\alpha_S = 4.85$, $\alpha_P = 9.27$, $\alpha_D = 4.26$, $\alpha_F = 4.33$, and $C_S = 1.53 \times 10^4$, $C_P = 2.36 \times 10^6$, $C_D = 1.22 \times 10^4$, and $C_F = 2.25 \times 10^4$, for the sharp, principal, diffuse, and fundamental series, respectively. The cross section for the leading member of each series is considerably larger than predicted by Eq. (8).

The shapes of all excitation functions follow a common behavior of rising rapidly from zero to a simple or multiple peak, following threshold, and then declining monotonically with energy throughout the rest of the investigated energy range. The details of this behavior vary among the different transitions. It is seen from Fig. 5 that the shapes of the members of a given spectral series resemble each other closely, which makes it possible to speak generally of the shapes of the sharp, principal, diffuse, and fundamental series. The exceptions to this pattern are the the lowest member(s) of each series, which rise less abruptly from threshold and have broader peaks than the upper members.

The sharp-series excitation functions have the most complex shape. This shape is characterized by a well-defined peak region several eV wide followed by a gradual decline between 15 and 50 eV. In the case of $6S$-$4P$, and presumably the others, the slope steepens beyond 50 eV, attaining an E^{-1} decline by about 200 eV. The peaks are double, the first in each case being a spike-shaped structure occurring immediately after onset. The apparent height and narrowness of this feature are evidently limited by the 0.75-eV energy resolution of the beam. Its position on the energy scale progresses steadily from 4.2 ± 0.2 eV in the case of $6S$-$4P$, to 5.0 ± 0.2 eV for $10S$-$4P$. In each case the second maximum is somewhat shorter and less defined than the first and occurs at about 1.5 eV higher. We do not observe a multiple-peak structure for the first member of the series ($5S$-$4P$); however, because of the inefficiency of the detector at the wavelength involved (12 432–12 522 Å), the signal is quite noisy and the peak structure may have been obscured.

The shape of the principal-series excitation functions is somewhat simpler in the sense that they fall off more uniformly with energy, possess-ing no points of inflection (on a log-log scale) beyond the peak. The peak region contains some detail but is not resolved into distinct maxima in our results. The $4P$-$4S$ cross section is the largest of all, has the lowest excitation potential, rises least steeply from onset, has the broadest maximum, and falls off the most slowly over an extended energy range. On its ascending portion, at about 2.4 ± 0.3 eV, it possesses a shoulder, i.e., an abrupt decrease in slope. At higher energies, up to 400 eV, the $4P$-$4S$ and $5P$-$4S$ excitation functions fall off less steeply than E^{-1}, in accordance with theoretical predictions.[23]

The diffuse-series shape is simpler than either of the two preceding in that it has only a single, uncomplicated peak. The lower members of the series, particularly $3D$-$4P$, are less sharply peaked than the upper members. All members fall off more steeply than those of the principal series. In the two cases investigated beyond 50 eV, i.e., $3D$-$4P$ and $5D$-$4P$, a rate of descent proportional to E^{-1} was attained beyond 200 eV.

The fundamental-series shape is similar to that of the diffuse series but falls off even more rapidly.

The similarity in shape from zero to 50 eV among excitation functions belonging to the same spectral series has already been noted. It is reasonable to suppose that this similarity continues in the higher-energy range as well, i.e., from 50 to 400 eV. With this assumption we can extend to 400-eV excitation functions that were actually measured only in the 0–50-eV interval. This is done by assigning to each such excitation function the higher-energy shape of a different member of the same spectral series—one for which measurements were made up to 400 eV. Thus the various members of the sharp series are assumed to have the same high-energy shapes as $Q_{6S\text{-}4P}$; the upper members of the principal and diffuse series are assumed to follow $Q_{5P\text{-}4S}$ and $Q_{5D\text{-}4P}$, respectively. In the case of the fundamental series no excitation function could be accurately measured at the higher energies because of the weakness of the signals. Within the 0–50-eV range, the behavior of the excitations functions approaches a E^{-1} variation. This is the same dependence that is expected, theoretically, in the high-energy limit.[24] On this basis we extend the fundamental-series excitation functions by joining them to an E^{-1} curve at 50 eV.

The extrapolated values obtained in this way are enclosed in parentheses in Table I and are indicated by a dashed curve in Fig. 5. Their precision is lower than that of the directly measured values but sufficient to form a basis of comparison with theory.

B. Error analysis

Beside the label for each transition in Table I is the overall experimental uncertainty in the optical excitation function, expressed as a percentage. A representative breakdown of an uncertainty, in terms of independent sources of error, is the following.

(i) 10% for number density. This is the same for all lines.

(ii) 7% for radiometric calibration. A somewhat larger value applies to the farthest ultraviolet and infrared lines.

(iii) 5% for the various transmittance and reflectance values, geometrical measurements of slit and aperture dimensions, beam-current measurements, and other sources of systematic error. This is approximately the same for all lines.

(iv) 5% for noise in the signal, for drifting of instruments, number density, etc. This is basically a reflection of the reproducibility of our results.

(v) 5% for the effects of anisotropy of excitation radiation, instrumental polarization, etc. This applies to a number of weaker lines in the principal, diffuse, and fundamental series, for which the "magic-angle polarizer" could not be used on account of signal weakness. This error source is energy dependent and could therefore lead to some distortion in excitation-function shapes.

These uncertainties are given with a confidence of 70%.

Although the total uncertainty in an absolute cross section may be 15%, the uncertainty in the ratio of any two cross section values—either for two different lines at the same energy or for the same line at two different energies—is considerably less. These ratios are not subject to uncertainty (i) and may have reduced susceptibility to several of the remaining errors, leaving a typical residual uncertainty of 10%.

A source of uncertainty that is peculiar to the $4P$-$4S$ cross section is the absorption of resonance radiation on its way out of the collision chamber. This problem can be eliminated by operating at a sufficiently low number density. However, as discussed in Sec. III, the accuracy of the number-density determination, using the resonance-transmission method, deteriorates at very low densities. Optimum precision of this measurement is achieved at densities at which 10% or more of the light from the resonance lamp is absorbed as it traverses the collision region, i.e., at densities of 1.4×10^{10} cm^{-3} and above. However, under these circumstances some of the $4P$-$4S$ electron-impact radiation must also be absorbed. Since this radiation has an escape path that is one-half as long as the

path traversed by the light from the resonance lamp (see Figs. 2 and 3), it is estimated that its degree of attenuation would be one-half as great, i.e., 5%. This is not strictly correct since the electron-impact radiation and the resonance-lamp radiation have slightly different Doppler widths and since the loss of electron-impact photons by scattering out of the detection cone is partially offset by the scattering into the detection cone of electron-impact photons originating in remote parts of the electron beam. But, despite the inexactness of this approximation, it cannot be in error by more than a few percent, i.e., much less than other experimental uncertainties. Thus we have simply increased our $4P$-$4S$ cross section, measured at the above-mentioned density, by 5%, to account for the effects of resonance scattering.

In addition to these uncertainties are others associated with the electron-energy scale. Calibration points exist at the various excitation thresholds of K I (1.6 to 4.3 eV) and K II (27 to 32 eV). The accuracy of the calibration is limited to about ±0.2 eV, primarily by uncertainties regarding the electron-energy distribution. The apparent shape of the ascending portion of each excitation function immediately following threshold (i.e., within 1 eV) is subject to distortion by the energy spread of the electron beam and therefore is of limited validity. Some local distortion of the energy scale is also possible as the ionization threshold is crossed[24] and space-charge neutralization by positive ions sets in; at the current densities used in our experiment this distortion could reach about 0.3 eV, leading to an overall uncertainty of ±0.35 eV. At higher energies the precision is limited to (1–2)% by the quality of the voltmeter.

C. Comparison with other experimental work

In comparing our experimental results for optical excitation functions with those of other workers, we consider first the excitation of the $4P$-$4S$ resonance line. This has been investigated in a number of previous experiments, the results of which are displayed along with ours in Fig. 7. The early results of Volkova and Devyatov[25] were obtained by using photographic detection in a single-beam—static-gas experiment, the number density being based upon standard vapor-pressure tables. Their values are the largest of the group by a wide margin and probably should be considered obsolete in view of the subsequent improvements in experimental methods, most notably the replacement of photographic detection by photoelectric detection. Nevertheless, the shape of
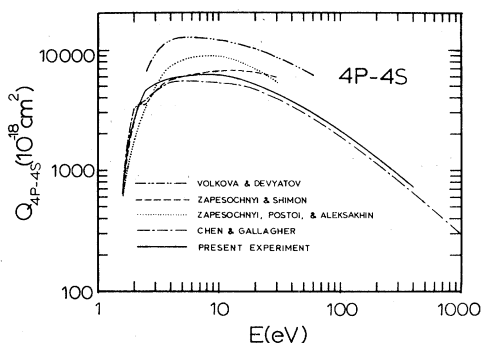
FIG. 7. Comparison of experimental results for $4P$-$4S$ optical excitation function.

their excitation function is consistent with later experiments, specifically ours and that of Chen and Gallagher.[11]

Chronologically, the next experiment was that of Zapesochnyi and Shimon,[26] who also used the single-beam–static-gas, equilibrium vapor-pressure method, but with a photomultiplier as a detector. Among the various experimental results for this excitation function, those of Zapesochnyi and Shimon are unique in the slowness with which they fall off with increasing impact energy. That work has since been superseded by a crossed-beam experiment by Zapesochnyi, Postoi, and Aleksakhin.[8] In the latter paper Zapesochnyi et al. attribute the unusual gradualness of the decline of the excitation function in the earlier work to the spurious effects of secondary electrons in the collision region. They attribute the differences in magnitude of the two results to faulty number-density determination and incorrect allowance for resonance-line absorption in the earlier work. We include both sets of data to be complete and to demonstrate the distorting effects of secondary electrons. Our own work does not confirm either of these two sets of data.

Over a broad energy range our $4P$-$4S$ excitation function agrees most closely with the result of a crossed-beam experiment by Chen and Gallagher.[11] Except at very low energies, i.e., below 2.4 eV, their curve, which is normalized to a modified version of the Born approximation, lies below ours by a fairly uniform amount, (7–14)%. Thus the difference between the two results is more a matter of normalization than of shape and the results are not incompatible in view of the 12% uncertainty we assign to our values (70% confidence).

The shoulderlike structure we observe at 2.4 $\pm$0.3 eV on the ascending portion of the $4P$-$4S$ excitation function has been noted by other experimenters.[8,11,27] Zapesochnyi and Shpenik[27] have
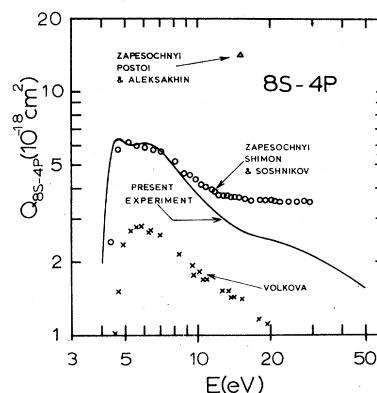

FIG. 8. Comparison of experimental results for $8S$-$4P$ optical excitation function.

resolved the structure into a subsidiary peak, which they locate at 2.1 eV. This feature suggests the existence of a K^- resonance in the vicinity, but the evidence from these experiments is not conclusive. The matter is better elucidated in the differential electron-scattering experiments of Eyb.[28] He examined the $4S$ and $4P$ differential cross sections for scattering angles 20° to 140°, in an energy interval of 2.0 to 3.2 eV, with a resolution of about 50 meV. He identified three resonance states (at 2.4, 2.6, and 2.68 eV) in this interval and attributed the complex post-threshold behavior of the $4P$ excitation function to these and to threshold effects caused by opening of the $5S$ (2.61 eV) and $3D$ (2.67 eV) channels.

Many of the other excitation functions have been examined over a restricted energy range by Volkova[29,30] and by Zapesochnyi et al.[8,27,31] For others, namely, the first members of the S and D series and the entire F series, the present measurements are the first reported.

Volkova's studies covered a dozen members of the S, P, and D series in the energy range 0–20 eV. She cited peak values in all cases and showed the energy dependence for a few members of the S and P series. A representative example is shown in Fig. 8. As a rule, her values are lower than ours (in contrast to the case with $4P$-$4S$) by factors of 2 to 10. They are almost certainly in error. The shapes are in approximate agreement with ours, although they have less detail. The initial ascending portion of her excitation functions appear to be shifted towards higher energies by a fraction of an eV relative to ours.

Zapesochnyi, Shimon, and Soshnikov[31] have measured a similar set of excitation functions from 0–30 eV. As in the case of $4P$-$4S$, the shapes they found differ from ours in the slowness with which they fall off with energy, as shown in Fig. 8. This behavior is probably

spurious—the result of the presence of secondary electrons in the collision region.[8] In many instances their cross-section values are in reasonable agreement with ours at the lower energies, but then diverge from ours as energy increases, probably because of the secondary-electron effect. In any case, Zapesochnyi *et al.* have remeasured a number of excitation functions and have reported new values for two of them, 8S-4P and 6D-4P, at 15 eV. As seen in Fig. 8, these more recent values are 3 to 4 times larger than the previous ones and are therefore at even greater variance with our own results.

The detailed peak structure we observe in the excitation functions of the upper sharp series, and to a lesser extent, the upper principal series, has not been noted by either Volkova[29,30] or Zapesochnyi, Shimon, and Soshnikov.[31] However, using an energy resolution of 0.4 eV (90% of all electrons), Zapesochnyi and Shpenik[27] have located several subsidiary maxima in the 5P-4S excitation function between 3.7 and 5.5 eV. The structures on the sharp-series excitation functions are suggestive of resonances but cannot be conclusively identified on the basis of our results.

V. DIRECT EXCITATION FUNCTIONS

The discussion thus far has been concerned with the excitation of spectral lines, a compound process composed of two elementary steps, namely, the direct electron-impact excitation of the various levels of the atom and the subsequent relaxation of the atom via radiative transitions between the levels. Experimentally, it is the combined excitation-plus-emission process that is most accessible. But the direct excitation process alone is of more fundamental interest and is better suited for theoretical treatment. In the remainder of this paper we will focus on the direct excitation process, characterized by the direct excitation functions $Q_j(E)$, which are defined as the cross sections for directly exciting atoms from the ground state to various excited states j by impact with electrons of energy E. From our experimentally measured optical excitation functions we will obtain a set of direct excitation functions. Theoretical calculations will then be discussed and a comparison made between our experimental and theoretical results.

A. Determination of experimental direct excitation functions from experimental optical excitation functions; additional uncertainties introduced

Each state j is populated by two means, namely, by direct impact excitation from the ground state and by radiative cascade from higher-lying levels.

It is depopulated only by the radiative decay to lower levels. There being no steady-state build-up of population in j, the rates of population and depopulation must balance. Since those rates are proportional to the corresponding cross sections, this requirement can be expressed by

$$Q_j(E) + \sum_{i>j} Q_{ij}(E) = \sum_{i<j} Q_{ji}(E). \qquad (9)$$

The first term on the left-hand side is the direct excitation function for j. The second term is the sum of the cascade into j from all higher levels i, and is called the cascade function for j. The sum on the right-hand side gives the total rate of depopulation of j and is termed the apparent excitation function of j.

Equation (9) permits the determination of $Q_j(E)$ in terms of the optical excitation functions of lines originating or terminating in j. Generally, it is not possible to measure all of these optical excitation functions, some of the lines lying in inaccessible parts of the spectrum. However, experimentally unobserved cross sections can be deduced from observed ones by making use of the fact that any two optical excitation cross sections with a common upper level stand in the same proportion as the corresponding transition probabilities. Thus, in making cascade corrections for a state j, any unobserved cascade from a level i, that is, Q_{ij}, can be expressed in terms of an observed cross section originating in i, that is, Q_{im}, according to

$$Q_{ij}(E) = (A_{ij}/A_{im})Q_{im}(E), \qquad (10)$$

where A_{ij} and A_{im} are the transition probabilities for $i \to j$ and $i \to m$. In determining the total of optical excitations originating in the state of interest, j, the same principle can be applied, yielding the following expression for the direct excitation functions for j,

$$Q_j(E) = \frac{1}{A_{jk}\tau_j} Q_{jk}(E) - \sum_{i>j} \frac{A_{ij}}{A_{im}} Q_{im}(E), \qquad (11)$$

where τ_j is the radiative lifetime of j, i.e., the reciprocal of the sum of all transition probabilities having j as an upper level. The first term on the right-hand side in Eq. (11) is the apparent excitation function for j, and the second term is the cascade into j. The apparent excitation function for j clearly has the same energy dependence as $Q_{jk}(E)$, and, to the extent that it dominates over the cascade function (second term on the right-hand side), this same shape will be taken by the resultant direct excitation function $Q_j(E)$. In this sense $Q_j(E)$ can be said to be derived from, or to correspond to, $Q_{jk}(E)$. In the case of a

large cascade function, $Q_j(E)$ can differ markedly in shape from $Q_{jk}(E)$, notwithstanding this terminology.

Equation (11) expresses the direct excitation function $Q_j(E)$ as a linear combination of directly measurable optical excitation functions, one originating in j and one in each state that supplies cascade into j. Reference to Fig. 1 shows that our finite set of experimental measurements of optical cross sections of the sharp, principal, diffuse, and fundamental series forms a sufficient data base, in conjunction with transition probability values available in the literature, for the determination of the direct cross sections for the lowest few S, P, D, and F levels (excluding $4F$), except that the cascade into $3D$ and $4D$ from $4F$, and into the various F levels from the G's, is unknown.

The direct excitation functions determined in this way from our experimental optical cross sections will be referred to subsequently as our "experimental direct excitation functions" although they depend upon the various transition probability values, many of which are of theoretical rather than experimental origin. The term "theoretical excitation functions" is reserved for calculated excitation functions, using the Born approximation, close-coupling approximation, etc.

We have taken transition probabilities from two sources. For the sharp, principal, and diffuse series we have used values from the critical compilation of Wiese, Smith, and Miles[19]; these values were based upon combined experimental and theoretical results were assigned maximum uncertainty values by the authors, ranging from 10% to 50%, and in one case more than 50%. For all other lines, i.e., for the fundamental series and for transitions between higher-lying levels, we have had to rely upon calculated values derived from semiempirical methods. Of three possible sources of these, Anderson and Zilitis,[32] Biemont and Grevesse,[33] and Lindgard and Nielsen,[34] we have chosen the last, which is the most recent and comprehensive. The choice among these three is not critical since they are based upon the same or similar methods of calculation and produce very similar results.

An estimate of the accuracy of Lindgard and Nielsen's results was not given by the authors. However, Wiese et al.[19] did estimate that for Anderson and Zilitis' values the uncertainty limit was within 50% and this estimate should apply equally to Lindgard and Nielsen's values, judging from the similarity of their results. The uncertainties assigned by Wiese et al. are presented by them as being the "limits of possible error" and thus evidently correspond to a rather high level of confidence. The standard deviation of the tabulated values from the true values would probably be much less than this. (Evidence supporting this interpretation is found in the experimental lifetime measurements of 18 S, P, and D states of sodium, done by Gallagher, Edelstein, and Hill.[35,36] The standard deviation between their results and those based upon Anderson and Zilitis' values is less than 10%, which is much smaller than the 25% estimated by Wiese et al. as the maximum possible error in Anderson and Zilitis' values for sodium.) On this basis, we have obtained transition probability uncertainties, corresponding to the 70% confidence level used elsewhere in this paper, by dividing the maximum-possible-error figures of Wiese et al. by 3. These uncertainties have then been combined with those in our experimental optical excitation functions in order to provide an estimate of uncertainty (70% confidence) in our experimental direct excitation functions. The transition probability uncertainties substantially degrade the excitation-function precision. The effect is most serious for those states from which considerable radiative branching occurs, in which case only a small portion of the radiation originating in the state is experimentally observed, the remainder having to be inferred by using the transition probabilities. An equivalent loss of precision occurs for states which are populated more by cascade than by direct excitation. In such cases there is significant cancellation between the apparent excitation and cascade functions, i.e., the two terms on the right-hand side of Eq. (11), thereby magnifying the fractional uncertainty in the direct excitation function.

A final element of uncertainty occurring in the transformation from optical to direct excitation functions results from the truncation of the series of terms representing cascade into a given level from successively higher levels. This error is mentioned for completeness only, for in practice the series converge quite rapidly, i.e., within a few terms, so that truncation errors probably do not exceed 2%.

B. Experimental results for direct excitation functions

We have carried out the conversion from optical to direct excitation functions for 14 excited states comprising the lowest four S, P, D, and F states, excepting $4F$ and $4D$. A sample breakdown of the conversion at an energy of 15 eV is shown in Table II. For each level the optical cross section for the transition originating in that level is given in the second column. Division of this figure by the radiative-branching ratio of the line

TABLE II. Experimental optical, apparent, cascade, and direct excitation cross sections of potassium.

| Level | Cross section (10^{-18} cm^2) at energy 15 eV | | | |
	Optical	Apparent	Cascade	Direct
5S	275	275	167	108
6S	26.1	41.1	21.9	19.2
7S	6.81	12.6	3.56	9.04
8S	2.69	5.50	0.88	4.62
4P	5690	5690	1210	4480
5P	43.1	255	81.5	173
6P	3.24	57.1	27.7	29.4
7P	0.43	14.5	5.76	8.74
3D	874	874	213 [a]	661 [a]
5D	8.87	40.3	8.06	32.3
6D	6.73	15.4	2.23	13.2
5F	21.4	27.8	3.9 [b]	23.9 [b]
6F	9.47	14.1	1.7 [b]	12.4 [b]
7F	4.88	7.86	0.75 [b]	7.11 [b]

[a] The cascade into 3D includes an estimated 104 units from 4F. The 3D direct cross section is corrected for this estimated cascade.

[b] The cascade into the F's includes no estimate of the contribution from the G's. The F direct cross sections are thus uncorrected for this cascade.

yields the apparent cross section, given in the third column. The sum of the cascade terms into the level is given in the fourth column, and the direct cross section, obtained by subtracting the cascade from the apparent cross section is given

in the last column.

Table III is a summary of our experimental direct excitation cross sections for the 14 states at selected energies. As has been mentioned, we have measured the optical excitation functions for only five transitions at energies above 50 eV. The direct cross sections associated with the upper levels of these five transitions are given in Table III by unbracketed values, beyond 50 eV. For the other nine levels, high-energy cross sections are enclosed in parentheses to emphasize the fact that they are dervied from extrapolated values. It is to be noted however that even the unbracketed values are not completely free of extrapolation errors since they involve the use of cascade functions which have been extrapolated to high energies.

The 14 experimental direct excitation functions, separated into four groups according to the orbital angular momentum, are plotted logarithmically in Fig. 9 with solid curves. The long-dashed curves represent extrapolations, in the sense just described for Table III, and the short-dashed curves are Born approximation calculations, to be discussed in Sec. VC. Figure 10 shows the experimental direct excitation functions of the four lowest-lying states on a linear scale (solid curve), along with theoretical values to be discussed in Sec. VC. It is seen from Fig. 9 that the direct excitation functions belonging to the same family, characterized by a given value of orbital angular momentum l, bear a resemblance

TABLE III. Experimental direct excitation functions of potassium.

| Level j | Uncertainty [a] (%) | Cross section Q_j (10^{-18} cm^2) at energy E(eV) | | | | | | | | |
		5	10	15	20	30	50	100 [b]	200 [b]	400 [b]
5S	50	323	168	108	91.0	85.9	57.8	(42.2)	(21.5)	(10.1)
6S	40	47.4	26.1	19.2	18.1	15.7	12.3	7.15	3.66	1.75
7S	30	22.1	13.2	9.04	8.09	6.79	5.24	(3.02)	(1.57)	(0.78)
8S	30	10.9	6.65	4.62	4.29	3.72	2.78	(1.51)	(0.79)	(0.39)
4P	15	4000	4660	4480	4150	3540	2860	1850	1140	663
5P	30	255	200	173	154	115	83.1	49.5	27.3	14.7
6P	40	48.2	32.9	29.4	26.6	20.3	13.1	(9.11)	(5.08)	(2.78)
7P	40	15.4	10.3	8.74	7.58	5.56	4.29	(2.56)	(1.42)	(0.77)
3D [c]	20	848	825	661	543	405	266	154	83.9	42.5
5D	40	67.0	44.6	32.3	25.4	17.9	12.0	6.62	3.47	1.73
6D	30	29.5	18.1	13.2	10.4	7.39	5.05	(2.72)	(1.43)	(0.72)
5F [d]	30	52.0	34.6	23.9	17.9	12.17	7.80	(4.04)	(2.01)	(1.00)
6F [d]	30	27.4	18.3	12.4	9.41	6.54	4.49	(2.10)	(1.05)	(0.52)
7F [d]	30	13.9	10.4	7.11	5.58	3.85	2.50	(1.22)	(0.61)	(0.30)

[a] Uncertainties correspond to a 70% confidence level.
[b] Values in parentheses are based upon extrapolation.
[c] The 3D excitation function has been corrected for an estimated amount of cascade from 4F.
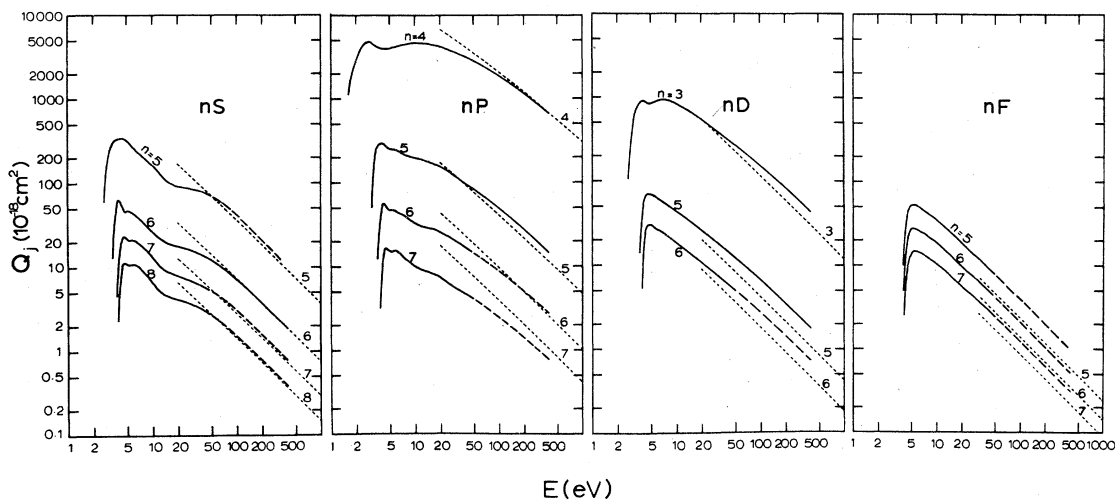[d] The F excitation functions have not been corrected for cascade from the G levels.

FIG. 9. Direct excitation functions of potassium for S, P, D, and F levels. The solid curves show the present experimental results; the long-dashed curves are extrapolations of these; the short-dashed curves are the present Born-approximation calculations. The $3D$ excitation function is based upon an estimated amount of the cascade from $4F$, explained in text. The various F excitation functions are not corrected for cascade from the G states.
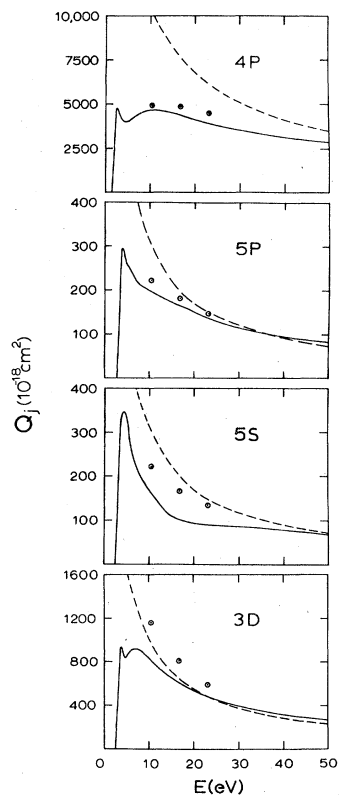

FIG. 10. Comparison of experimental and theoretical direct excitation functions for the four lowest-lying states, $4P$, $5P$, $5S$, and $3D$. The solid curves show the present experimental results, the dashed curves the present Born calculations, and the circles indicate the 15-state close-coupling calculations.

to one another and they decrease regularly in magnitude with increasing principal quantum number n. As in the case of optical excitation functions already discussed, the direct excitation cross sections for fixed l and impact energy E, but varying n, can be fit to a power law in n_{nl}^{*}, the effective quantum number. However, such a fit excludes the lowest-lying member of each family, as well as Q_{4D}, leaving only two or three cross sections in each family. This is too few to be conclusive so we do not present the results for the curve-fitting parameters.

Each of the excitation functions is unique in some way so we discuss them individually below, emphasizing sources of error and the reliability of the results and making comparisons with the experimental results of other workers, where possible. We begin with the particularly important case of $4P$ and then take up the remaining states in the order S, P, D, and F.

1. 4P state

Q_{4P} is the largest and most accurately determined of all the experimental direct excitation functions. Its high accuracy stems from three separate circumstances: (i) that Q_{4P-4S}, from which it is derived, is the most accurate of all optical excitation functions, (ii) that there is no radiative branching (i.e., unobserved transition) from $4P$, and (iii) that the cascade into $4P$ is not too large, and, more importantly, is directly observed, since it consists of the sharp and diffuse

spectral series, i.e.,

$$Q_{4P} = Q_{4P-4S} - \sum_{n \geq 5} Q_{nS-4P} - \sum_{n \geq 3} Q_{nD-4P}. \quad (12)$$

Thus this cross section has no dependence upon any calculated transition probabilities, with their concomitant errors. Moreover, the cascade measurements, for the most part, extend to 400 eV, so that there is little dependence upon energy-extrapolated cascade. Thus the conversion from optical to direct excitation function for the 4P level introduces little additional uncertainty and the final precision of Q_{4P} is about 15%.

A dip in the 4P direct excitation function between 2 and 10 eV (Fig. 9) is revealed when the comparatively sharply peaked cascade functions from S and D levels are subtracted from the broad, featureless 4P-4S optical excitation function. This kind of structure has been found in the 3P direct excitation function of sodium by Enemark and Gallagher.[9] The precision of the experimental data is sufficient to ensure that this feature is not merely an artifact of inaccurate cascade analysis. Independent evidence for a portion of this shape is found in the inelastic electron-scattering data of Eyb,[28] which shows the 4P differential cross section to be declining with energy over the range of his experiment, 2.2 to 3.2 eV, at all angles covered, from 20° to 140°.

Korchevoi and Przonski[37] have measured the 4P direct excitation function in the energy range between 1.6 and 2.4 eV, using the trapped-electron method, with an energy resolution of 0.15 eV. In the higher part of this range their results are about 25% lower than ours. As the energy is reduced towards the 4P threshold (1.61 eV) the accuracy of our results deteriorates, owing to the energy inhomogeneity of our beam, and a comparison of experimental values is of little significance.

In an electron-scattering experiment Williams and Trajmar[38] have measured the relative differential cross sections for the 4S, 4P, and 5S + 3D (unresolved) channels, at scattering angles between 5° and 140°, and at energies of 6.7, 16, and 60 eV. These were integrated over all angles and the resulting relative integral cross sections were normalized at each energy by setting their sum equal to the difference between the total cross section, as measured by Kasdan, Miller, and Bederson,[39] and the ionization cross section, as measured by Korchevoi and Przonski[37] and by McFarland and Kinney.[40] Their results for the 4P excitation cross section at 6.7, 16, and 60 eV are 3070, 3110, and 2440×10⁻¹⁸ cm² with an uncertainty of 50%. These values are somewhat

lower than our own (4300, 4450, and 2500×10⁻¹⁸ cm², respectively) but are not incompatible in view of the cited uncertainties.

Hertel and Ross[41,42] have measured differential-scattering cross sections for the 4P, 5S, 3D, 5P, 6S + 4D (unresolved), 4F and 6P channels at several energies between 40 and 200 eV. Their measurements were made at one angle only, 0°, and thus provide little quantitative information about the integral cross sections of interest in the present paper. While a comparison of their differential forward cross sections with our integral cross sections is difficult to interpret, it can be noted that such a state-by-state comparison reveals a considerable degree of correlation between the two quantities.

2. 5S state

This state, more than any other, is populated primarily by cascade from higher levels, predominantly 5P. Thus the direct cross section is the difference between two comparably sized quantities [see Eq. (9)] with independent errors and its precision suffers accordingly. Even though there is no radiative branching from 5S to add further uncertainty, the precision of this cross section is the worst of the entire set, 50%.

A comparison of Fig. 5 with Fig. 9 shows the significant difference in shape between the optical and direct excitation functions caused by the subtraction of cascade.

3. 6S state

There is considerable radiative branching from 6S, as well as a rather large, poorly known cascade from 6P; thus the final precision of Q_{6S} is about 40%, not much better than for Q_{5S}.

The peak occurring immediately after threshold, at about 4 eV, is more sharply defined in Q_{6S} than in Q_{6S-4P}. It rises above the second peak, at 4.0 eV, by almost 40% and would probably be much higher if observed with better beam-energy resolution. As in the case of 5S, the influence of the cascade upon the excitation-function shape is quite pronounced.

4. 7S and 8S states

These levels both have radiative branching comparable to that of 6S; the cascade is less significant, however, and the final precision is correspondingly improved to about 30%. The excitation-function shapes are little influenced by the cascade.

5. 5P state

There is considerable radiative branching in this case, the observed line, 5P-4S, accounting for only about one-sixth of the total radiation from 5P. Fortunately, the branching ratio is more accurate than most because of the accuracy with which the 5P-4S transition probability[19] and the 5P lifetime[43] are known. This advantage is somewhat offset by the high uncertainty in the cascade from 4D. Overall precision is 30%.

6. 6P and 7P states

There is a large degree of branching from these levels, only 6% (for 6P) and 3% (for 7P) of the total radiative decay occurring in the observed lines. The precision of the optical excitation functions is lower than most and cascade is substantial. Thus the final precision is poor, about 40%.

The detailed structure on Q_{6P} and Q_{7P} between 4 and 20 eV is very sensitive to variations in the cascade corrections and is thus of limited validity.

7. 3D state

Several factors are conducive to good precision in determining Q_{3D}. Those are the absence of branching from 3D and the smallness of the cascade from the P's and the upper F's. Moreover, the latter cascade was directly measured, since it corresponds to the fundamental spectral series. The remaining cascade, i.e., the unobserved Q_{4F-3D}, had to be estimated. Guided by the systematic trends of our experimental optical excitation functions within the various spectral series (see Sec. IV A), we approximated Q_{4F-3D} by multiplying our measured Q_{5F-3D} by a factor of 5, and displacing the resulting curve towards lower energies, to give the correct threshold energy. There is some arbitrariness in this approach but since this cascade is responsible for only about 12% of the total population of 3D, considerable latitude is possible in its estimation without seriously increasing the uncertainty in Q_{3D}. The final precision is about 20%. We notice a double-peak structure in Q_{3D} similar to that of Q_{4P}. The exact shape of the peak region is sensitive to the cascade function including the estimated Q_{4F-3D}, and is therefore somewhat uncertain.

8. 4D state

The observed line, 4D-4P, accounts for only a very small fraction, perhaps 1%, of the total radiation from 4D, owing to the anomalously small 4D-4P transition probability. This transition probability is very poorly known,[19] values

given for it in the literature ranging over a factor of ten.[32,44] The precision of the 4D apparent excitation function is correspondingly poor and the matter is further aggravated by the large, uncertain cascade from higher P and F levels. The final result for the 4D direct cross section is of such uncertainty as to be almost meaningless and is therefore not presented.

9. 5D and 6D states

There is considerable branching from these levels. However, the cascade is not large, and the final value for the experimental direct excitation function is probably correct within (30-40)%.

10. 5F, 6F, and 7F states

Most of the radiation from these levels is in the fundamental spectral series and is therefore directly observed in our experiment. The cascade from the D levels is not large, typically accounting for about 10% to 15% of the total rate of population of the F states. The cascade from the G levels occurs in the infrared and is not accessible to our experiment; it was estimated by means of Born calculations of the excitation functions of several G states, which were assigned Coulomb wave functions. These calculations indicate that the cascade from the G states is smaller than that from the D states and thus does not contribute greatly to the total rate of F-level population. These results are only approximate and we did not incorporate them quantitatively into our cascade analysis for the F states. Thus the values cited for experimental F direct excitation functions in Tables II and III and in Fig. 9 actually represent the F direct excitation function plus the unknown, but evidently small, cascade from the G levels. The precision is 30%.

11. Total inelastic-scattering cross section

Summing up the direct excitation cross sections for all excited states yields the total inelastic cross section for the neutral potassium atom. The same result may be obtained more simply, however, by summing up the optical excitation functions of the principal series alone, i.e.,

$$Q_{TI} = \sum_j Q_j = \sum_{n \geq 4} Q_{nP-4S} . \qquad (13)$$

This follows from the fact that each event of direct electron-impact excitation is followed by a sequence of deexciting radiative transitions, the terminal transition belonging to the principal series. From Table I it is seen that the first member, Q_{4P-4S}, accounts for about 99% of the

sum of excitation function of the principal series. Thus the total inelastic cross section is nearly identical to Q_{4P-4S}. It is not subject to errors in transition probabilities, cascade, etc., so its final precision is the same as for Q_{4P-4S}, namely, 12%.

C. Comparison with theory

The energy range 0–400 eV can be divided into several intervals according to the theoretical models and approximations best suited for computation of excitation cross sections. With some arbitrariness we define these intervals as follows: high energy, beyond 50 eV; medium energy, 10 to 50 eV; low evergy, threshold to 10 eV. Our discussion of theoretical calculations and their comparison with our experimental results will be divided into separate sections corresponding to these intervals. In addition to the theoretical works cited in these sections, there appear in the literature a number of papers on the theoretical calculation of excitation cross sections of K using different methods and covering different energy ranges. A summary of these calculated results has been given by Chen and Gallagher.[11] They also provide a graphical display for the comparison of the different sets of cross sections.

1. High energy: Born approximation

At high energies, the well-known Born approximation is the most suitable theoretical approach and, indeed, has been used as a standard against which to normalize experimental results for relative excitation functions. We have computed Born cross sections for excitation of 16 states of potassium, namely, $5S \cdots 8S$, $4P \cdots 7P$, $3D \cdots 6D$, and $4F \cdots 7F$. The calculation, which makes use of Hartree-Fock-Slater wave functions for the potassium atom, has been described by Korff.[45] An earlier set of calculations for 11 states (5S–7S, 4P–7P, and 3D–6D) was done by Vainshtein, Opykhtin, and Presnyakov.[46] The agreement between the two sets of calculations is fairly good, the rms difference being 13%. Greene and Williamson[14] have made a Born calculation for the 4P state; in addition they used the Bethe and Ochkur approximations to perform calculations for the same 11 states considered by Vainshtein et al. Greene and Williamson's calculations agree with our own to within 6% rms, except for the cases of 4D and 5D, where their values are lower than ours (and Vainshtein's) by (30–70)%. Evidently, the major source of these discrepancies is in the wave functions employed, as will be discussed shortly.

A summary of our Born calculations for the 16

TABLE IV. Coefficients A_j and B_j in the asymptotic form of the Born approximation of the direct excitation function of potassium. $Q_j(E) = A_j E^{-1} + B_j E^{-1} \log_{10} E$. The units are 10^{-18} cm^2 for the cross sections and eV for energy.

Level j	A_j	B_j
5S	3 750	0
6S	755	0
7S	286	0
8S	146	0
4P	12 000	97 000
5P	2 880	588
6P	812	73
7P	356	20
3D	11 800	0
4D	1 410	0
5D	411	0
6D	179	0
4F	400	0
5F	227	0
6F	135	0
7F	85	0

states is given in Table IV. Since the Born approximation is valid only at high energies, we cite only the high-energy asymptotic form,[23]

$$Q_j(E) = A_j E^{-1} + B_j E^{-1} \log_{10} E . \qquad (14)$$

With the tabulated values of A_j and B_j this form represents our Born cross sections with a precision of 2% or better at energies above 100 eV.

For purposes of comparing theory with experiment we have included our Born-approximation excitation functions in Fig. 9 along with our experimental values. It will be seen from Fig. 9 that, as higher energies are approached, the experimental and the Born-theoretical excitation functions attain the same energy dependence, so that for each state the ratio of theoretical to experimental cross sections approaches a constant value. For 4P the ratio appears to be unity; the close agreement here is significant since for this state both the experimental and theoretical results are expected to be of optimum reliability. For the remaining P states the high-energy Born values are within 25% of experimental values in the rms sense. For the S series the agreement is quite good, theory and experiment never differing by more than 10% at high energies. In the case of the D and F states, however, there is considerably greater disparity, with theoretical values consistently lying below experimental values by 30% to 45%. The degree and regularity of this discrepancy is greater than we would ex-

pect on the basis of systematic experimental er-
rors alone (primarily number-density determina-
tion and radiometric calibration), even including
uncertainties in our energy-extrapolation proced-
ure and our neglect of the cascade from the G
levels into the F's. Thus it seems likely that a
significant portion of the discrepancy originates
elsewhere, most likely in the transition probabil-
ity values adopted or in our Born calculations.
For example, systematic differences of the order
of 10% between experimental and theoretical
radiative lifetimes, such as are indicated for Na
by the measurements of Gallagher, Edelstein,
and Hill,[35,36] could, when used in Eq. (11), lead
systematically to somewhat magnified errors,
perhaps 20%, in our experimental direct excita-
tion functions.

The uncertainty in the transition probabilities
renders the comparison between our Born-theo-
retical and experimental direction excitation func-
tions somewhat ambiguous. The $4P$ cross sec-
tion, as mentioned in Sec. V B 1, is exceptional
in being independent of the transition probabilities,
and in that case the close agreement between ex-
periment and Born theory is significant. The
total inelastic cross section too is independent of
the transition probabilities (Sec. V B 11), but
since it is so heavily dominated by Q_{4P} a com-
parison of theory and experiment for this case
yields little additional information beyond what
has already been supplied by a comparison of the
theoretical and experimental values of Q_{4P} alone.
However, subtracting Eq. (12) from Eq. (13)
yields a relationship between direct and optical
excitation functions that is independent of transi-
tion probabilities and involves neither Q_{4P} nor
Q_{4P-4S}, i.e.,

$$\sum_{\substack{\text{all } j \\ \text{except } 4P}} Q_j$$

$$= \sum_{n \geq 5} Q_{nP-4S} + \sum_{n \geq 5} Q_{nS-4P} + \sum_{n \geq 3} Q_{nD-4P}. \qquad (15)$$

This expresses the cross section for exciting all
states except $4P$ as a sum of the directly mea-
sured optical cross sections for the entire sharp,
principal, and diffuse series, excepting Q_{4P-4S}.
Inserting Born-theoretical direct cross section
values in the left-hand side of Eq. (15) and experi-
mental optical cross sections in the right-hand
side we find that, in the high-energy limit, the
theoretical cross section sum is 25% below the
experimental. This is somewhat larger than the
estimated experimental uncertainty of 15%–20%,
suggesting that the sum of the Born cross sections,
which is dominated by the $3D$, $5S$, and $5P$ states,
may be too small in the high-energy limit.

A likely source of error is in the Hartree-Fock-
Slater atomic wave functions used in our Born
calculation. A degree of optimization of these
wave functions is achieved by adjusting the statis-
tical-exchange parameter so as to reproduce the
observed energy levels. This procedure, how-
ever, does not necessarily optimize the accuracy
of the ground-state and excited-state wave func-
tions in regions where they overlap each other,
which is critical to the calculation of the excita-
tion cross sections. The ground-state wave func-
tions obtained by the Hartree-Fock-Slater scheme
are generally quite accurate, but we are less cer-
tain about the accuracy of the excited-state Har-
tree-Fock-Slater wave functions in the inner re-
gion. In the case of the $4P$ state, we find that
the calculated $4S$-$4P$ oscillator strength using the
Hartree-Fock-Slater wave functions agrees with
experiment[19] to within 2%, and this partially con-
firms the accuracy of the $4P$ function. Such tests
are not as conclusive with the other states since
the appropriate oscillator strengths are not known
to sufficient precision. The cross sections of
these states may be quite sensitive to wave-func-
tion variations. We note that some of the states
for which the disparity between experimental and
theoretical cross sections is the greatest, i.e.,
$4D$ (not shown because of extreme uncertainty),
$5D$, and $6D$, are the same states for which Born-
type cross sections reported by different research
groups are also in the greatest disagreement
among themselves,[14] presumably because of the
wave functions. For the F states we are not
aware of any alternative published Born calcula-
tions with which to compare our values. In test-
ing the sensitivity of the calculated cross sections
to the choice of wave functions for these states
we have found that the substitution of Coulomb
wave functions for the Hartree-Fock-Slater wave
functions raises the Born cross sections by,
typically, 30%–40%. The same result is obtained
for the G states. The conclusion is that wave-
function inaccuracies could be responsible for a
considerable portion of the discrepancy between
our high-energy experimental and Born-theoreti-
cal direct excitation functions.

2. Intermediate energy: close-coupling theory

To extend the validity of the theoretical calcula-
tions of the excitation cross sections to lower
incident energies, we apply the method of close
coupling (multistate). Here the distortion of the
incident wave by the target atom is taken into
account so that the high-energy restriction asso-
ciated with the Born approximation is relaxed.
The use of a multistate manifold also allows for

the indirect coupling of the initial with the final state via some of the intermediate states. The general procedure has been described in an earlier work[47] on close-coupling calculations of electron excitation of Na and therefore will not be given in detail here. We determine the target wave functions by the Hartree-Fock-Slater self-consistent-field procedure and expand the composite wave function of the projectile-target system by the target-electron eigenfunctions. The coefficients of expansion, which are functions of the projectile coordinates, are determined by solving a series of coupled differential equations numerically. The infinite expansion (by the target states), in practice, must be truncated. It includes, in addition to the initial (i) and final (f) states, a number of intermediate states which can provide important coupling modes other than $i \rightarrow f$. We check the convergence of the expansion by monitoring the calculated values of excitation cross sections as additional target states are included. To limit the scope of the computational work we neglect the exchange interaction between the projectile and target electrons. This approximation becomes serious at very low energies so our calculation is not carried below 10 eV. This defines qualitatively an intermediate-energy range in which the Born approximation is no longer valid and yet exchange is not expected to play a dominant role. The nonexchange, multistate close-coupling scheme is, of course, still applicable above the intermediate-energy domain but the results presumably would approach the Born cross sections. Furthermore, at high energies, the partial waves corresponding to large angular momenta contribute more significantly to the cross sections, making the close-coupling calculation more lengthy and less rewarding. We have performed a series of two-state, three-state, 10-state, and 15-state close-coupling calculations at 10.52-, 16.8-, and 23.1-eV incident energies, and the results for three representative states are discussed in the following paragraphs.

As in the case of Na,[47] there exists for K an extraordinarily strong coupling between the ground state ($4S$) and the first resonant excited state ($4P$). This results in a gross overestimation of the $4P$ cross section by the Born approximation at energies below 30 eV because of the neglect of the $4P$-$4S$ back coupling and the coupling of $4P$ with other states. Indeed a two-state ($4S$-$4P$) close-coupling calculation, which allows for the back coupling, drastically decreases the cross sections. For instance, at a 10.52-eV incident energy the Born and two-state close coupling cross sections are 101×10^{-16} and 70.0×10^{-16} cm^2, respectively.

As for the coupling of $4P$ with states other than $4S$, by far the strongest one is the $4P$-$3D$. Inclusion of $3D$ in the close-coupling expansion allows the intense $4P$-$3D$ coupling to funnel the $4S$-$4P$ coupling to the $3D$ state, leading to a suppression of the $4P$ cross sections. Thus at 10.52 eV our $4S$-$4P$-$3D$ three-state close-coupling calculation for the $4P$ cross section gives 51.9×10^{-16} cm^2, which is substantially smaller than the two-state value. To test the effects of the higher states we performed a 10-state calculation covering the $4S$, $4P$, $3D$, $4D$, $4F$, $5S$, $5P$, $5D$, $5F$, and $6P$ states and a 15-state one with $4S$, $4P$, $3D$, $4D$, $4F$, $5S$, $5P$, $5D$, $5F$, $6S$, $6P$, $6D$, $6F$, $7P$, and $8P$; the $4P$ cross sections at 10.52 eV so obtained are 50.0 and 49.4×10^{-16} cm^2, respectively. The three-state expansion is seen to converge well and there is virtually no difference between the 10-state and 15-state results. The same kind of covergence is also found at incident energies of 16.8 and 23.1 eV.

In general, the strongest couplings are found between two states whose l quantum numbers differ by one unit. Thus, for excitation to the $3D$ state, the $4S$-$3D$ coupling is not of such strength as to cause overestimation by the Born approximation. On the other hand, since the $4S$-$4P$ and $3D$-$4P$ couplings are both much stronger than $4S$-$3D$, inclusion of the indirect coupling between $4S$ and $3D$ via the $4P$ state may significantly alter the $3D$ cross sections. This is confirmed by a comparison of the cross sections calculated by the Born approximation and by the $4S$-$4P$-$3D$ three-state close coupling; at 10.52 eV these are, respectively, 9.66×10^{-16} and 14.2×10^{-16} cm^2. Upon augmenting the basis manifold to 10 and 15 states, these cross sections change into 11.7×10^{-16} and 11.6×10^{-16} cm^2, respectively. The reduction in cross section from the three-state to 10-state calculation indicates that the effect of the $4S$-$3D$ indirect coupling via $4P$ is counteracted to some degree by similar linkages via some of the higher states. (The same kind of partial cancellation has been found in the $3D$ excitation cross sections of Na for which the seven-state cross section at 10.52 eV lies about midway between the Born and the $3S$-$3P$-$3D$ three-state values.[47]) Convergence in the close-coupling expansion is confirmed by the close agreement between the 10-state and 15-state cross sections.

For the $5S$ state the Born approximation gives 2.97×10^{-16} cm^2 at 10.52 eV, as compared with 2.50×10^{-16} and 2.33×10^{-16} cm^2, respectively, from 10-state and 15-state close coupling. While there is still a 10% difference between the 10-state and 15-state values, we believe that the latter to be quite close to convergence because all the states that couple strongly with $5S$ have

been included in the expansion. Unlike the case of 3D, the multistate close-coupling cross sections for 5S are smaller than the Born value. Such a difference in behavior between the S and D states has been found for Na in the close-coupling work of Korff et $al.$, and an explanation has been given in their paper.[47]

One can, in principle, obtain from the 15-state calculation the cross sections for all the 14 excited states included. However, as we move on to the higher excited states, the question of convergence becomes a more serious one. For the 5P and 4D states the 10-state and 15-state cross sections are quite close but convergence tests for the higher states generally cannot be made with a comparable degree of certainty. Thus in Table V we list only the 4P, 5P, 5S, 3D, and 4D states.

For the purpose of comparison we display in Fig. 10 the close-coupling (15 states) cross sections for the 4P, 5P, 5S, and 3D states along with the experimental direct excitation functions. Included therein are also the Born-approximation results (dashed curves). The agreement between theory (close coupling) and experiment is very good for the 4P state. Especially impressive is the vast "correction" furnished by the method of close coupling to the Born cross sections below 20 eV. The 5P state shows similar behavior in that the close-coupling cross sections agree well with experiment and are lower than the Born values. For the 5S state the close-coupling cross sections are well above the experimental curve. The difference is within our estimated 50% experimental uncertainty for 5S at 10.5 and 23.1 eV, but exceeds 50% at 16.8 eV. The close-coupling calculation does not well reproduce the shape of the observed excitation function; however, it does come somewhat closer to experiment than does the Born approximation. The 3D state differs from 4P, 5P, and 5S in that the close-coupling cross sections move farther away from experiment as compared with the Born approximation. The discrepancy is well beyond the 20%

precision range that is assigned to the 3D experimental data. Also the close-coupling cross sections, as compared with the experimental data, appear to increase too steeply at low energies. Since we are not able to make a reliable determination of the 4D direct cross section from our experimental data, no comparison of close-coupling to experimental values can be made for this state.

The theoretical cross sections obtained from the method of close coupling at the intermediate-energy region for the 4P and 5P states are in good agreement with experiment but are less satisfactory for the 5S and 3D states. The disagreement could be due to, at least in part, inaccurate wave functions, as we have suggested in our discussion of the Born approximation. Another possible cause for the discrepancy found in 3D and 5S is the neglect of the projectile–target-electron exchange in the close-coupling calculation. For electron excitation involving no change in the target spin quantum number, the direct electrostatic interation of the incident electron with the target certainly plays a much more important role than the exchange terms at intermediate energies, yet the latter may still have an appreciable influence on the excitation cross sections at incident energies as high as several times the threshold energy. For example, in a recent close-coupling calculation for the $X^1\Sigma_g^+ \rightarrow B^1\Sigma_u^+$ excitation in H_2,[48] inclusion of the exchange effect is found to cause an appreciable decrease in the cross sections from the nonexchange calculation up to 60 eV, the difference being about 18% at 35 eV. Hence it is reasonable to expect a lowering of the calculated cross sections by taking exchange into account. The degree of lowering may vary from one state to another. For the 4P state the 4S-4P coupling is so intense that the cross sections are in the saturation region, i.e., do not depend sensitively on the coupling strength. This means that the exchange potential may not have much effect on $4S \rightarrow 4P$ excitation. The

TABLE V. Comparison of Born-approximation and 15-state close-coupling calculations of direct excitation cross sections of potassium.

Level j	Direct excitation cross section Q_j (10^{-18} cm^2) at E(eV)					
	10.5 eV		16.8 eV		23.1 eV	
	Born approximation	15-state close coupling	Born approximation	15-state close coupling	Born approximation	15-state close coupling
4P	10 200	4960	7600	4880	6100	4510
5P	300	222	206	182	157	147
5S	297	223	199	167	150	135
3D	966	1160	630	812	473	597
4D	129	193	80	115	59	81

$4S$-$5S$ and $4S$-$3D$ Coulomb couplings, on the other hand, are much weaker; consequently, inclusion of the exchange terms may alter the cross section in a more significant way.

3. Low energy

In the low-energy region the most elaborate close-coupling calculation in the literature is the one for $4P$ excitation at 1.6–5.0 eV reported by Moores using a three-state manifold.[49] His approach differs from the one we just described for the intermediate-energy region in that the former used a semiempirical-model potential to describe the target states and included projectile–target-electron exchange for the lower partial waves. In the range of 2.5 to 5.0 eV each of Moores' values agree with our experimental $4P$ cross sections within 10%, although detailed structure of our $4P$ experimental excitation function is not indicated in his results. At 2.0 eV and below, our experimental results are less valid, owing to the finite energy resolution of the beam, so a comparison with Moores' calculation would not be useful.

VI. EXPERIMENTAL RESULTS FOR POLARIZATION AND DIRECT EXCITATION FUNCTIONS OF MAGNETIC SUBLEVELS OF 4P

We have examined the polarization of the resolved components of the $6S$-$4P$, $4P$-$4S$, $3D$-$4P$, and $5D$-$4P$ doublets and the unresolved $5P$-$4S$ and $5F$-$3D$ doublets. The $6S$-$4P$ doublet and the $4P_{1/2}$-$4S_{1/2}$ line of the $4P$-$4S$ doublet were found to be unpolarized, within experimental error, in accordance with theoretical predictions.[1] For the other lines the polarization as a function of energy follows a common behavior. This is characterized by a steady decline of the polarization function, starting at a fairly large, positive value near threshold, then passing through zero at some energy between 10 and 35 eV, and finally attaining a negative, slowly varying (perhaps asymptotic) value at higher energies. (In the convention used here the polarization is positive if the stronger componet of the electric vector is parallel to the electron beam and negative if perpendicular to it.) The polarization at or very near to threshold could not be accurately measured because of the steepness of the excitation functions there and the finite energy resolution of the electron beam.

Our most reliable results are for the $4P$-$4S$ and $3D$-$4P$ transitions, which have the shortest lived upper levels (26 nsec for $4P$ and 38 nsec for $3D$) and are thus the least susceptible to depolarization by stray magnetic fields. The results for
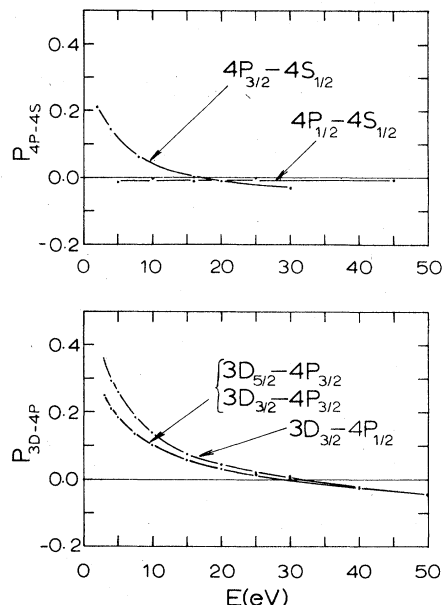

FIG. 11. Experimental polarization of $4P$-$4S$ and $3D$-$4P$ lines.

these transitions are shown in Fig. 11.

The $4P$-$4S$ measurements were made at a low density, 2.3×10^{10} cm^{-3}, in order to reduce the depolarizing effects of resonance-line scattering. At this density the signal is weak and consequently the error in the polarization measurement could be as high as 3%. Our $4P_{3/2}$-$4S_{1/2}$ polarization function is qualitatively in agreement with that of Chen and Gallagher,[11] i.e., the overall shapes are similar and the energy at which the polarization passes through zero is in agreement within about 1 eV. However, our values exceed theirs in magnitude by an amount which is greater than might be expected on the basis of the experimental uncertainties cited. Our results appear to be consistent with a theoretical threshold value of 23.5% computed according to the procedure given by Flower and Seaton[50]; the agreement is not wholly conclusive, however, for our results cannot be extrapolated back to threshold with certainty considering the possibility of irregular behavior there.

As seen from Fig. 11, the $3D$-$4P$ doublet, particularly the $3D_{3/2}$-$4P_{1/2}$ line, is somewhat more strongly polarized than the $4P$-$4S$ doublet and the polarization crossses zero at a higher energy, about 30 eV. These measurements were made at a density of 6×10^{12} cm^{-3}.

From our measurements of the excitation and polarization functions of the $4P$-$4S$ lines we have determined the apparent excitation function (i.e., direct plus cascade) of the individual magnetic

substates of $4P_{3/2}$ and $4P_{1/2}$ by applying the theory of Percival and Seaton[13] and Flower and Seaton,[50] which takes account of the hyperfine structure and radiative lifetime of the $4P$ levels. These apparent excitation functions were then corrected for cascade, which comes almost entirely from $5S$ and $3D$. In this step we used the $5S$-$4P$ and $3D$-$4P$ optical excitation and polarization functions in conjunction with standard dipole-radiation formulas,[18] neglecting hyperfine structure for simplicity, to determine the cascade into the various magnetic substates of $4P$. The results of this analysis, carried out in the coupled representation (L, S, J, M_J), are the experimental direct excitation functions for the M_J substates of $4P_{1/2}$ and $4P_{3/2}$. For convenience in interpreting these results and comparing them to theory we have transformed to the uncoupled representation (L, S, M_L, M_S). In this representation there are only two different excitation functions of $4P$, corresponding to $|M_L| = 0$ and $|M_L| = 1$, since the excitation process is symmetric in M_L and M_S. These two constituent excitation functions are related to the total $4P$ direct excitation function by

$$Q_{4P} \equiv \sum_{M_L, M_S} Q_{4P_{M_L, M_S}} = 2Q_{4P_{0,1/2}} + 4Q_{4P_{1,1/2}}. \quad (16)$$

They are displayed graphically in Fig. 12, with solid curves.

They are seen to exhibit strikingly different behavior. For $|M_L| = 0$ the excitation function has a high, narrow peak near threshold, followed by a steady monotonic decline with increasing energy. For $|M_L| = 1$ the excitation function is much smaller near threshold, rising slowly and some-

FIG. 12. Experimental direct excitation functions of magnetic sublevels of the $4P$ states. The cross sections are symmetric in M_L and M_S, so that $Q_{4P} = 2Q_{4P_{0,1/2}} + 4Q_{4P_{1,1/2}}$.

what unevenly to a broad maximum between 15 and 20 eV. Thus in the immediate post-threshold region the $4P$ excitation is almost exclusively to the $M_L = 0$ substates, while at about 15 eV each M_L, M_S substate is equally excited. Also shown in Fig. 12 are the 15-state close-coupling results at 10.5, 16.8, and 23.1 eV, connected by dashed lines. Over this limited range the theoretical and experimental results are seen to be in reasonable agreement as regards the general shape of the excitation functions and the value of the impact energy at which $|M_L| = 0$ and $|M_L| = 1$ substates are equally excited.

VII. CONCLUDING REMARKS

After a systematic study of electron-impact excitation for the various states of the K atom it is instructive to discuss these results as a whole in relation to the current framework of our knowledge on electron-atom excitation derived from earlier works. We will address this point from two angles. The first one focuses on qualitative properties such as the shape of excitation functions and the relative magnitude of cross sections. The second stage is on a more quantitative level with reference to theoretical calculations.

As a reference point for qualitative discussion of the excitation data, we turn to the prototypical case of helium, for which extensive measurements have been reported from numerous laboratories over the last few decades. Many of the features observed in K are in accord with those found for He. For instance, excitation functions of states of the same L quantum number all have similar shape (except for the lowest member) and an optically allowed state has larger excitation cross sections and a broader excitation function as compared to forbidden states of the same principal quantum number. On the other hand, the alkalimetal atoms have their unique features. An important one is the exceptionally large cross section of the first resonant state—much larger than, for example, the $2\,^1P$ cross section of He. From the theoretical standpoint this can be traced to the unusually strong coupling between $4S$ and $4P$. This strong coupling also causes the Born approximation to overestimate the $4P$ cross section in the intermediate-energy range. The deviation of the observed cross sections from the Born values is smaller for $5P$ because of the weaker $4S$-$5P$ coupling. This provides an explanation for the anomalous shape of the $4P$ excitation function in the intermediate-energy range, which differs significantly from the higher P states. For K we are able to measure the excitation functions of the F states which have not been
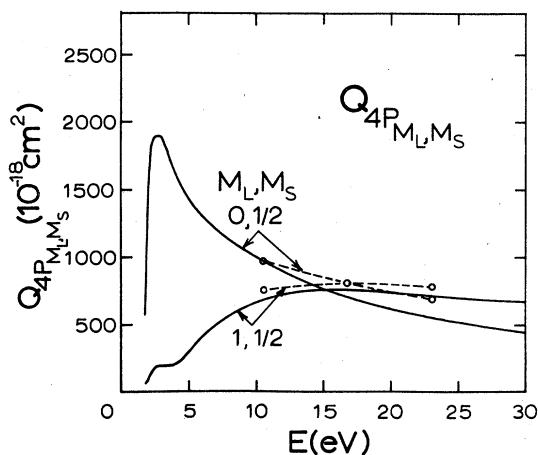
reported for He. At high energies one expects the same $1/E$ dependence for both the D and F states. However, our measurements show that the D and F excitation functions have very similar shape even at low energies.

For high-energy electron excitation the Born approximation is expected to be reliable; indeed the Born cross sections generally show satisfactory agreement with the measured values, although the discrepancy for some of the D and F states is somewhat larger than the experimental uncertainty. This could be due to the approximate nature of the wave functions employed in the calculation. Theoretical calculations for excitation cross sections at the intermediate energies are much more difficult and systematic studies with comparison to experiment are sparse in the literature. An effort in this direction is made in this paper by using the method of close coupling. A complete close-coupling calculation at an incident energy well above the threshold is extremely complex. In the work reported here special emphasis is placed on understanding how the cross sections are influenced by indirect coupling through intermediate states. This entails solving many-channel scattering equations and to make the computation tractable we neglect exchange between the incident and target electrons. The results of these multistate close-coupling calculations (10–25 eV) are in excellent agreement with experiment for the $4P$ and $5P$ states, but much larger discrepancies are found in the cases of $5S$ and $3D$. The nonexchange close-coupling calculation enables us to identify the important intermediate states for $5S$ and $3D$ excitation; thus it may be possible to improve the calculation by using more accurate wave functions and incorporating projectile-target exchange, with fewer states included in the multistate expansion. It should also be interesting to perform similar test of close-coupling calculations for other alkali-metal atoms. In view of the very favorable results for the two P states (especially $4P$, for which the experimental data is the most accurate), further efforts to develop the method of close coupling into a practical tool for cross-section calculation in the intermediate-energy region should be particularly worthwhile.

*Present address: Dept. of Physics, San Diego State Univ., San Diego, Calif. 92182.

†Present address: 17 Longmeadow Rd., Portsmouth, R. I. 02871.

[1] B. L. Moiseiwitsch and S. J. Smith, Rev. Mod. Phys. 40, 238 (1968). Note erratum concerning polarization in Rev. Mod. Phys. 41, 574 (1969).

[2] R. M. St. John, F. L. Miller, and C. C. Lin, Phys. Rev. 134, A888 (1964).

[3] H. R. Moustafa Moussa, F. J. De Heer, and J. Schutten, Physica 40, 517 (1969).

[4] F. A. Sharpton, R. M. St. John, C. C. Lin, and F. E. Fajen, Phys. Rev. A 2, 1305 (1970).

[5] J. K. Ballou, C. C. Lin, and F. E. Fajen, Phys. Rev. A 8, 1797 (1973).

[6] R. D. Cowan and K. L. Andrew, J. Opt. Soc. Am. 55, 502 (1965).

[7] W. Christoph, Ann. Phys. (Leipzig) 23, 51 (1935).

[8] I. P. Zapesochnyi, E. N. Postoi, and I. S. Aleksakhin, Zh. Eksp. Teor. Fiz. 68, 1724 (1975) [Sov. Phys. JETP 41, 865 (1976)].

[9] E. A. Enemark and A. Gallagher, Phys. Rev. A 6, 192 (1972).

[10] D. Leep and A. Gallagher, Phys. Rev. A 10, 1082 (1974).

[11] S. T. Chen and A. C. Gallagher, Phys. Rev. A 17, 551 (1978).

[12] J. C. DeVos, Physica 20, 690 (1954). An alternative source is R. D. Larrabee, J. Opt. Soc. Am. 49, 619 (1959).

[13] I. C. Percival and M. J. Seaton, Philos. Trans. R. Soc. A 251, 113 (1958).

[14] T. J. Greene and W. Williamson, Jr., At. Data Nucl. Data Tables 14, 161 (1974).

[15] R. Hultgren, P. D. Desai, D. T. Hawkins, M. Gleiser, K. K. Kelley, and D. D. Wagman, Selected Values of the Thermodynamic Properties of the Elements (American Society for Metals, Metals Park, Ohio, 1973).

[16] A. N. Nesmeyanov, Vapor Pressure of the Elements (Academic, New York, 1963).

[17] A. C. G. Mitchell and M. W. Zemansky, Resonance Radiation and Excited Atoms (Cambridge University, London, 1971).

[18] E. U. Condon and G. H. Shortley, The Theory of Atomic Spectra (Cambridge University, Cambridge, 1970).

[19] W. L. Wiese, M. W. Smith, and B. M. Miles, Atomic Transition Probabilities, Natl. Stand. Ref. Data Ser., Natl. Bur. Stand. No. 22 (U. S. GPO, Washington, D.C., 1969), Vol. II.

[20] E. C. Wang and J. Yellin, Phys. Rev. A 4 838 (1971).

[21] E. Arimondo, M. Inguscio, and P. Violino, Rev. Mod. Phys. 49, 31 (1977).

[22] D. G. Hummer, Mem. R. Astron. Soc. 70, 1 (1965).

[23] M. Inokuti, Rev. Mod. Phys. 43, 297 (1971).

[24] D. W. O. Heddle and R. G. W. Keesing, in Advances in

Atomic and Molecular Physics, edited by D. R. Bates and I. Esterman (Academic, New York, 1968), Vol. IV.

[25]L. M. Volkova and A. M. Devyatov, Isv. Akad. Nauk SSSR, Ser. Fiz. 27, 1052 (1963).

[26]I. P. Zapesochnyi and L. L. Shimon, Opt. Spektrosk. 21, 261 (1966) [Opt. Spectrosc. 21, 155 (1966)].

[27]I. P. Zapesochnyi and O. B. Shpenik, Zh. Eksp. Teor. Fiz. 50, 890 (1966) [Sov. Phys. JETP 23, 592 (1966)].

[28]M. Eyb, J. Phys. B 9, 101 (1976).

[29]L. M. Volkova, Opt. Spektrosk. 6, 273 (1959) [Opt. Spectrosc. 6, 179 (1959)].

[30]L. M. Volkova, Opt. Spektrosk. 13, 849 (1962) [Opt. Spectrosc. 13, 482 (1962)].

[31]I. P. Zapesochnyi, L. L. Shimon, and A. K. Soshnikov, Opt. Spektrosk. 19, 864 (1965) [Opt. Spectrosc. 19, 480 (1965)].

[32]E. M. Anderson and V. A. Zilitis, Opt. Spektrosk. 16, 177 (1964) [Opt. Spectrosc. 16, 99 (1964)].

[33]E. Biemont and N. Grevesse, At. Data Nucl. Data Tables 12, 217 (1973).

[34]A. Lindgard and S. E. Nielsen, At. Data Nucl. Data Tables 19, 533 (1977).

[35]T. F. Gallagher, S. A. Edelstein, and R. M. Hill, Phys. Rev. A 11, 1504 (1975).

[36]T. F. Gallagher, S. A. Edelstein, and R. M. Hill, Phys. Rev. A 14, 2360 (1976).

[37]Y. P. Korchevoi and A. M. Przonski, Zh. Eksp. Teor. Fiz. 51, 1617 (1966) [Sov. Phys. JETP 24, 1089 (1967)].

[38]W. Williams and S. Trajmar, J. Phys. B 10, 1955 (1977).

[39]A. Kasdan, T. Miller, and B. Bederson, Phys. Rev. A 8, 1562 (1973).

[40]R. H. McFarland and J. D. Kinney, Phys. Rev. 137, A1058 (1965).

[41]I. V. Hertel and K. J. Ross, J. Phys. B 1, 697 (1968).

[42]I. V. Hertel and K. J. Ross, J. Phys. B 2, 285 (1969).

[43]R. H. Schmieder, A. Lurio, and W. Happer, Phys. Rev. 173, 76 (1968).

[44]E. F. M. Van der Held and J. H. Heierman, Physica 3, 31 (1936).

[45]D. F. Korff, Ph.D. thesis, University of Wisconsin, 1973 (unpublished).

[46]L. A. Vainshtein, V. Ophkhtin, and L. Presnyakov, P. N. Lebedev Institute of Physics Report No. A-53 (unpublished). A summary of these results, amended by private communication, is given in Ref. 1.

[47]D. F. Korff, S. Chung, and C. C. Lin, Phys. Rev. A 7, 545 (1973).

[48]S. Chung and C. C. Lin, Phys. Rev. A 17, 1874 (1978).

[49]D. L. Moores, J. Phys. B 9, 1329 (1976).

[50]D. R. Flower and M. J. Seaton, Proc. R. Soc. London 91, 59 (1967).